Midlatitude Cloud Radiative Effect Sensitivity to Cloud Controlling Factors in Observations and Models: Relationship with Southern Hemisphere Jet Shifts and Climate Sensitivity

KEVIN M. GRISE[a] AND MITCHELL K. KELLEHER[a]

[a] *Department of Environmental Sciences, University of Virginia, Charlottesville, Virginia*

(Manuscript received 19 December 2020, in final form 21 April 2021)

ABSTRACT: An effective method to understand cloud processes and to assess the fidelity with which they are represented in climate models is the cloud controlling factor framework, in which cloud properties are linked with variations in large-scale dynamical and thermodynamical variables. This study examines how midlatitude cloud radiative effects (CRE) over oceans covary with four cloud controlling factors—midtropospheric vertical velocity, estimated inversion strength (EIS), near-surface temperature advection, and sea surface temperature (SST)—and assesses their representation in CMIP6 models with respect to observations and CMIP5 models. CMIP5 and CMIP6 models overestimate the sensitivity of midlatitude CRE to perturbations in vertical velocity and underestimate the sensitivity of midlatitude shortwave CRE to perturbations in EIS and temperature advection. The largest improvement in CMIP6 models is a reduced sensitivity of CRE to vertical velocity perturbations. As in CMIP5 models, many CMIP6 models simulate a shortwave cloud radiative warming effect associated with a poleward shift in the Southern Hemisphere (SH) midlatitude jet stream, an effect not present in observations. This bias arises because most models' shortwave CRE are too sensitive to vertical velocity perturbations and not sensitive enough to EIS perturbations, and because most models overestimate the SST anomalies associated with SH jet shifts. The presence of this bias directly impacts the transient surface temperature response to increasing greenhouse gases over the Southern Ocean, but not the global-mean surface temperature. Instead, the models' climate sensitivity is correlated with their shortwave CRE sensitivity to surface temperature advection perturbations near 40°S, with models with more realistic values of temperature advection sensitivity generally having higher climate sensitivity.

KEYWORDS: Extratropics; Cloud radiative effects; General circulation models

1. Introduction

Properly representing clouds and their radiative effects remains one of the biggest challenges of climate modeling. It is well established that cloud feedbacks are responsible for the majority of the spread in the equilibrium climate sensitivity (i.e., the steady-state global-mean surface temperature response to doubled atmospheric carbon dioxide concentrations) across models (e.g., Bony et al. 2006; Dufresne and Bony 2008; Vial et al. 2013; Webb et al. 2013; Zelinka et al. 2020). Efforts to constrain the spread in equilibrium climate sensitivity (ECS) across models have largely focused on the role of low cloud feedbacks over tropical and subtropical ocean basins (e.g., Bony and Dufresne 2005; Qu et al. 2014, 2015; Myers and Norris 2016; Klein et al. 2017; McCoy et al. 2017). However, the role of extratropical cloud feedbacks in determining ECS has recently been gaining more attention, as Zelinka et al. (2020) linked the higher average climate sensitivity of models from phase 6 of the Coupled Model Intercomparison Project (CMIP6) to decreased extratropical low cloud coverage and albedo.

One of the most effective ways to understand cloud processes and to assess the fidelity with which they are represented in models is to use the cloud controlling factor framework. In this framework, large-scale dynamical and thermodynamical environmental variables are identified that strongly covary with observed cloud properties, allowing a direct comparison between how observed and model clouds respond to perturbations in environmental factors. This approach has been widely used to understand cloud variability and feedbacks over tropical and subtropical oceans (Norris and Iacobellis 2005; Myers and Norris 2013, 2015, 2016; Qu et al. 2014, 2015; Seethala et al. 2015; McCoy et al. 2017; Klein et al. 2017; Scott et al. 2020), and has been more recently applied to understand clouds over extratropical oceans (Grise and Medeiros 2016, hereafter GM16; Wall et al. 2017; Zelinka et al. 2018; Kelleher and Grise 2019; Scott et al. 2020).

In the extratropics, four key cloud controlling factors are midtropospheric vertical velocity, estimated inversion strength (EIS), near-surface temperature advection, and sea surface temperature (SST) (see also Scott et al. 2020). Midtropospheric ascent is associated with enhanced cloud fraction in the mid-to-upper troposphere (Weaver and Ramanathan 1997; Li et al. 2014; Wall et al. 2017), such as the nimbostratus and high-topped convective clouds that occur within the warm sector of extratropical cyclones (Lau and Crane 1995, 1997; Gordon et al. 2005). A strong temperature inversion (EIS) above the marine boundary layer favors the development of low-level stratocumulus clouds (Klein and Hartmann 1993; Wood and Bretherton 2006), as the strong inversion inhibits mixing of drier free tropospheric air into the moist marine boundary layer. Advection of cold air over warmer sea surface temperatures also promotes

Supplemental information related to this paper is available at the Journals Online website: https://doi.org/10.1175/JCLI-D-20-0986.s1.

Corresponding author: Kevin M. Grise, kmg3r@virginia.edu

DOI: 10.1175/JCLI-D-20-0986.1

enhanced low cloud cover by increasing sensible and latent heat fluxes from the ocean surface into the atmosphere (Norris and Iacobellis 2005; Zelinka et al. 2018; Miyamoto et al. 2018). In contrast, increases in SST may decrease low cloud cover, as warmer SSTs strengthen the moisture contrast between the marine boundary layer and the overlying free troposphere and consequently increase the effectiveness of mixing dry free tropospheric air into the moist marine boundary layer (Rieck et al. 2012; Frey and Kay 2018). However, the influence of SSTs on low cloud cover is stronger in the subtropics than at midlatitudes, where there is less of a moisture contrast between the boundary layer and free troposphere (Kawai et al. 2017; Scott et al. 2020).

One common application of these cloud controlling factor relationships is to estimate cloud feedbacks in a warming climate [see review by Klein et al. (2017)]. By multiplying the observed sensitivity of cloud properties to the cloud controlling factors (as estimated from interannual variability) by the expected changes in the cloud controlling factors with climate change, one can derive an observational estimate of cloud feedbacks. This approach inherently assumes that the sensitivity of cloud properties to the cloud controlling factors is time scale invariant (i.e., the sensitivity remains approximately the same on interannual and climate change time scales), and that the changes in the cloud controlling factors with climate change are relatively well constrained by models. A similar approach can be used to reconstruct model cloud feedbacks, multiplying the model sensitivity of cloud properties to the cloud controlling factors (as estimated from interannual variability) by the expected changes in the cloud controlling factors with climate change (e.g., Qu et al. 2015). Applying this approach, previous studies have found that the bulk of the uncertainty in model cloud feedbacks lies in the sensitivity of cloud properties to the cloud controlling factors (which depends strongly on model cloud parameterizations), rather than in the response of the cloud controlling factors to climate change (Qu et al. 2014; Myers and Norris 2016; Klein et al. 2017). This motivates a need to examine the intermodel spread in the sensitivity of cloud properties to the cloud controlling factors, to assess improvements across model generations, and to identify consistent model biases against observations.

In this study, we focus on examining the observed and modeled sensitivity of top-of-atmosphere shortwave cloud radiative effect (CRE)[1] to cloud controlling factors, with a strong emphasis on the Southern Hemisphere (SH) midlatitudes (30°–60°S). This emphasis is motivated by the finding of Zelinka et al. (2020), who find larger shortwave cloud feedbacks in CMIP6 models (on average) than in CMIP5 models (the previous generation of global climate models), with the largest differences occurring over the 30°–60°S latitude band. In CMIP5 models, the shortwave radiative effects of midlatitude clouds were overly sensitive to midtropospheric vertical velocity perturbations when compared to observations (GM16; Kelleher and Grise 2019). In contrast, CMIP5 models' sensitivities of shortwave CRE and low cloud cover to perturbations in EIS and near-surface temperature advection were underestimated (GM16; Zelinka et al. 2018; Kelleher and Grise 2019).

A key consequence of these biases in CMIP5 models was a systematic misrepresentation of cloud radiative effects associated with variability in the midlatitude atmospheric circulation. For example, many CMIP5 models simulate a net shortwave warming effect when the midlatitude jet stream and its associated large-scale ascent and mid-to-high topped clouds shift poleward, as the clouds reflect less sunlight back to space as they move to higher latitudes (e.g., Boucher et al. 2013; Grise et al. 2013; Grise and Polvani 2014, hereafter GP14). However, observations show little evidence of a net shortwave warming effect associated with a poleward jet shift in most midlatitude ocean basins, as low cloud cover often increases in the region vacated by the storm-track clouds (Ceppi and Hartmann 2015; GM16; Zelinka et al. 2018). An erroneous feedback occurs in many CMIP5 models because they do not properly capture the sensitivity of midlatitude low clouds to the increases in EIS and near-surface cold advection that occur in the region vacated by the storm-track clouds (GM16; Zelinka et al. 2018). It remains unknown whether the representation of these processes has improved in CMIP6 models.

CMIP5 models also struggled to properly capture the observed thermodynamic sensitivity of midlatitude clouds. In these models, the optical depth of midlatitude low clouds was too sensitive to temperature perturbations (Gordon and Klein 2014; Terai et al. 2016), at least in part because of an improper partitioning between ice and liquid in mixed-phase clouds (McCoy et al. 2016; Tan et al. 2016). In CMIP6 models, Zelinka et al. (2020) found a weaker sensitivity of midlatitude low cloud cover and liquid water path to SST perturbations, resulting in an average increase of low cloud cover and liquid water path with warming in CMIP5 models but little SST sensitivity in CMIP6 models. This was hypothesized to be due to an increase in mean-state supercooled liquid water in CMIP6 models (Zelinka et al. 2020).

The purpose of this paper is to compare and contrast the sensitivity of midlatitude shortwave CRE in CMIP5 and CMIP6 models to the four cloud controlling factors introduced above (midtropospheric vertical velocity, EIS, near-surface temperature advection, and SST), and to assess any model improvements relative to observations. Specifically, we focus our discussion on whether the intermodel spread in the shortwave CRE sensitivity to the cloud controlling factors is helpful in explaining the intermodel spread in 1) the cloud radiative effects associated with meridional shifts in the SH midlatitude jet stream and 2) ECS.

2. Data and methods

The primary data used in this study are monthly mean output from the 28 CMIP5 models listed in Table 1 (WCRP 2011; Taylor et al. 2012) and the 34 CMIP6 models listed in Table 2 (Eyring et al. 2016; WCRP 2019). We selected this subset of models, as they had documented values of ECS in the published literature (Meehl et al. 2020; Zelinka et al. 2020) and

[1] Shortwave cloud radiative effect is defined as the difference in outgoing top-of-atmosphere shortwave radiation between clear-sky and all-sky scenes (e.g., Ramanathan et al. 1989).

TABLE 1. Listing of the CMIP5 models used in this study. Following Grise and Polvani (2014), the jet-CRE index is defined using the regression coefficients in Fig. 5 averaged over 30°–60°S (as plotted in Fig. 5d). Models with a positive index are denoted as type I, and models with a negative index are denoted as type II. Asterisks denote models that were classified as type II by Grise and Polvani (2014), but whose jet-CRE indices are positive.

Model name	Jet-CRE index ($W\,m^{-2}$)	Model type
ACCESS1.0	−0.34	II
ACCESS1.3	−0.36	II
BCC-CSM1.1	1.01	I
BCC-CSM1.1(m)	0.75	I
BNU-ESM	1.38	I
CanESM2	0.72	I
CCSM4	0.43	I
CNRM-CM5	0.21	I
CSIRO-Mk3.6.0	−0.78	II
FGOALS-g2	0.55	I
FGOALS-s2	0.81	I
GFDL CM3	−0.25	II
GFDL-ESM2G	−0.67	II
GFDL-ESM2M	−0.51	II
GISS-E2-H	0.36	I
GISS-E2-R	0.31	I
HadGEM2-ES	−0.28	II
INM-CM4	−0.21	II
IPSL-CM5A-LR	0.75	I
IPSL-CM5A-MR	0.79	I
IPSL-CM5B-LR	0.37	I*
MIROC5	0.01	I*
MIROC-ESM	1.55	I
MPI-ESM-LR	0.46	I
MPI-ESM-MR	0.62	I
MPI-ESM-P	0.39	I
MRI-CGCM3	−0.14	II
NorESM1-M	0.63	I

TABLE 2. As in Table 1, but for the listing of the CMIP6 models used in this study.

Model name	Jet-CRE index ($W\,m^{-2}$)	Model type
ACCESS-CM2	−0.28	II
ACCESS-ESM1-5	−0.42	II
AWI-CM-1-1-MR	0.59	I
BCC-CSM2-MR	0.25	I
BCC-ESM1	1.05	I
CAMS-CSM1-0	0.30	I
CESM2	−1.00	II
CESM2-WACCM	−1.09	II
CNRM-CM6-1	0.10	I
CNRM-CM6-1-HR	0.01	I
CNRM-ESM2-1	0.06	I
CanESM5	0.63	I
E3SM-1-0	−0.62	II
EC-Earth3	−0.43	II
EC-Earth3-Veg	−0.40	II
FGOALS-f3-L	0.32	I
GISS-E2-1-G	0.44	I
GISS-E2-1-H	0.39	I
GISS-E2-2-G	0.28	I
HadGEM3-GC31-LL	−0.15	II
HadGEM3-GC31-MM	−0.20	II
INM-CM4-8	−0.20	II
INM-CM5-0	−0.13	II
IPSL-CM6A-LR	0.00	I
KACE-1-0-G	−0.35	II
MIROC-ES2L	0.82	I
MIROC6	0.06	I
MPI-ESM1-2-HR	0.51	I
MPI-ESM1-2-LR	0.76	I
MRI-ESM2-0	0.11	I
NESM3	0.81	I
NorESM2-LM	−1.13	II
SAM0-UNICON	−0.35	II
UKESM1-0-LL	−0.05	II

included all necessary variables for the analyses presented. We use 200 years of the preindustrial control run of each model to estimate the sensitivity of shortwave CRE to month-to-month variability in the midlatitude cloud controlling factors. To examine the climate change response, we also make use of the abrupt $4xCO_2$ runs from each model, in which atmospheric carbon dioxide concentrations are quadrupled and then held fixed for the duration of a 150-yr-long run.

We compare the model results with the sensitivity of shortwave CRE to month-to-month variability in the midlatitude cloud controlling factors derived from observations. To do this, we use monthly mean shortwave top-of-atmosphere radiative fluxes from the CERES Energy Balanced and Filled (EBAF) version 4.1 dataset (Loeb et al. 2018; CERES Science Team 2020) to calculate shortwave CRE, monthly-mean SSTs from the Hadley Centre Sea Ice and Sea Surface Temperature dataset (HadISST: Met Office Hadley Centre 2000; Rayner et al. 2003), and monthly-mean wind, temperature, and humidity data from the ERA5 reanalysis (ECMWF 2017; Hersbach et al. 2020) to calculate the remaining cloud controlling factors. We examine the observations over the period 2001–18.

To provide further physical interpretation for our results, we also make brief use of observed cloud fraction from the International Satellite Cloud Climatology Project (ISCCP). Following GM16, we use the simulator-oriented ISCCP cloud product produced for the Cloud Feedback Model Intercomparison Project (CFMIP) to aid in model evaluation (CFMIP 2011; Pincus et al. 2012; Zhang et al. 2012), which is available from July 1983 to June 2008. Low cloud fraction derived from passive satellite measurements is complicated by the fact that low clouds are often obscured by the presence of clouds at higher altitudes. Therefore, we use the random overlap assumption (Morcrette and Fouquart 1986; Weare 2000) to estimate the actual observed low cloud fraction L':

$$L' = L/(1 - M - H), \tag{1}$$

where L, M, and H are the low (cloud-top pressure > 680 hPa), middle (440 hPa $<$ cloud-top pressure $<$ 680 hPa), and high (cloud-top pressure $<$ 440 hPa) cloud fractions from ISCCP, respectively.

In this study, we focus on four midlatitude cloud controlling factors: 500-hPa vertical velocity (ω_{500}), EIS, near-surface

temperature advection (TADV), and SST. Following Wood and Bretherton (2006), EIS is calculated as

$$\mathrm{EIS} = \mathrm{LTS} - \Gamma_m^{850}(z_{700} - \mathrm{LCL}), \tag{2}$$

where LTS (lower tropospheric stability) is the potential temperature difference between the surface and 700 hPa ($\theta_{700} - \theta_{\mathrm{sfc}}$), Γ_m^{850} is the moist adiabatic lapse rate at 850 hPa, z_{700} is the altitude of the 700-hPa level, and LCL is the altitude of the lifting condensation level [determined using the method of Georgakakos and Bras (1984)]. Near-surface temperature advection is calculated as $-\mathbf{V}_{925} \cdot \nabla\mathrm{SST}$, where $\mathbf{V}_{925}$ is the 925-hPa wind vector and ∇SST is the sea surface temperature gradient (calculated using spherical coordinates).

We define the sensitivity of shortwave CRE to month-to-month variations in the four midlatitude cloud controlling factors (CCFs) using the regression coefficients $\partial\mathrm{CRE}'/\partial\mathrm{CCF}'$ from the following multiple linear regression model:

$$\begin{aligned}\Delta\mathrm{CRE} = &\left(\frac{\partial\mathrm{CRE}'}{\partial\omega_{500}'}\right)\Delta\omega_{500} + \left(\frac{\partial\mathrm{CRE}'}{\partial\mathrm{EIS}'}\right)\Delta\mathrm{EIS}\\ &+ \left(\frac{\partial\mathrm{CRE}'}{\partial\mathrm{TADV}'}\right)\Delta\mathrm{TADV} + \left(\frac{\partial\mathrm{CRE}'}{\partial\mathrm{SST}'}\right)\Delta\mathrm{SST}\\ &+ \text{residual},\end{aligned} \tag{3}$$

where the primes denote deviations from the mean seasonal cycle. The regression coefficients from univariate linear regression models based on each cloud controlling factor individually are qualitatively similar at midlatitudes, but differ substantially in the tropics and subtropics (where month-to-month variability among the four cloud controlling factors is more strongly correlated). Other studies have used additional cloud controlling factors, such as near-surface wind speed and free-tropospheric relative humidity, in multiple linear regression models focused on low clouds (e.g., Qu et al. 2015; Scott et al. 2020). Here, we find that the adjusted r^2 value (which measures the value of adding predictors to a multiple linear regression model) does not notably increase with the addition of surface wind speed as a predictor for shortwave CRE (particularly at midlatitudes), suggesting that a wind speed predictor does not provide significant added value to our regression model. If we add free-tropospheric relative humidity as a predictor, variance inflation factors (which measure multicollinearity among predictors in a multiple linear regression model) increase substantially, producing a regression model with less reliable and less stable estimates of the regression coefficients. For these reasons, we do not include surface wind speed and free-tropospheric relative humidity as predictors in Eq. (3).

We define the latitude of the SH midlatitude jet using the latitude of the maximum in the monthly mean 850-hPa zonal-mean zonal wind field. The jet latitude is calculated using the Tropical-width Diagnostics code package (TropD; Adam et al. 2018a,b), using the ''peak'' option in the function TropD_Metric_EDJ.

We evaluate statistical significance using a standard two-tailed Student's t test. As a stricter test of statistical significance on geographical maps where regression and correlation coefficients are calculated at individual grid points, we also employ the Wilks (2016) procedure to control the false discovery rate of multiple simultaneous hypothesis tests. On all maps, fine stippling indicates significance via a standard Student's t test, and bold stippling indicates significance via the Wilks (2016) methodology.

3. Sensitivity of shortwave CRE to midlatitude cloud controlling factors

We begin by reviewing the global sensitivities of shortwave CRE to variations in the four midlatitude cloud controlling factors. To do this, in Fig. 1, we examine regressions of monthly anomalies of shortwave CRE onto monthly anomalies of each of the four cloud controlling factors, where the term anomalies refers to variations about the mean seasonal cycle. The regressions are computed separately at each grid point using the multiple linear regression model described above [see Eq. (3)]. We focus on the global oceans, as additional controlling factors are relevant over land. The left column of Fig. 1 shows the observed sensitivities, the center column shows the multimodel-mean sensitivities for CMIP5 models, and the right column shows the multimodel-mean sensitivities for CMIP6 models. The sensitivities are plotted for a one standard deviation anomaly in each cloud controlling factor at each grid point (as defined from observations); the sensitivities unscaled by standard deviation are shown in the online supplemental material (see Fig. S1 therein).

Figures 2–4 provide additional information to support the interpretation of Fig. 1. Figure 2 shows the multimodel mean biases in CMIP5 and CMIP6 models relative to observations, as well as any significant difference in the biases in CMIP6 models relative to CMIP5 models. Figure 3 plots the weighted averages of the regression coefficients from Fig. 1 over all oceanic grid points within the 30°–60°S band, where the regression coefficient at each grid point is weighted by the cosine of latitude. Figure 4 shows the corresponding sensitivities of observed high and low cloud fraction to the four midlatitude cloud controlling factors. The cloud fraction sensitivities for the models are qualitatively similar, but are not shown here because only a small (nonrepresentative) subset of the models provide the satellite simulator output necessary to directly compare model cloud fraction with observations. For reference, analogous plots to Figs. 1–3 for longwave CRE are also provided in the supplemental material (Figs. S2–S4).

The observed sensitivity of shortwave CRE to 500-hPa vertical velocity variations is positive nearly everywhere globally (Fig. 1a; see also Fig. 6a of GM16), indicating that upward vertical velocity anomalies (negative anomalies of ω_{500}) are associated with increased reflection of shortwave radiation by clouds (negative anomalies of shortwave CRE). This relationship primarily reflects variations in high-topped free-tropospheric cloud cover with vertical velocity (Fig. 4a). The observed sensitivity is largest in the deep tropics and decays toward midlatitude oceans. Over the stratocumulus zones of the eastern subtropical ocean basins, there are small regions where the observed sensitivity is near zero, indicating that vertical velocity plays a lesser role in governing cloud cover in these regions compared to the other cloud controlling factors

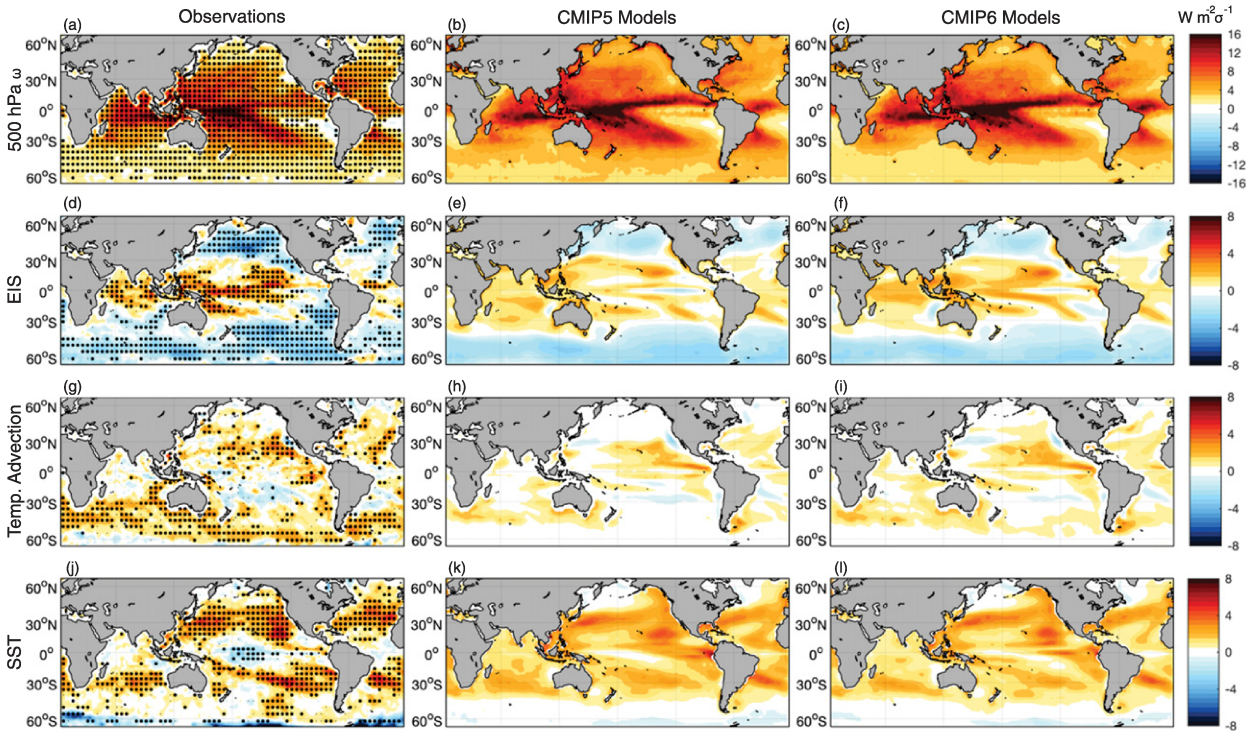

FIG. 1. Regressions of monthly shortwave CRE anomalies onto monthly anomalies in four cloud controlling factors [following Eq. (3)]: (a)–(c) 500-hPa vertical velocity (ω), (d)–(f) estimated inversion strength (EIS), (g)–(i) near-surface temperature advection, and (j)–(l) sea surface temperature (SST). Results are shown for (left) 2001–18 CERES shortwave CRE anomalies regressed on cloud controlling factor anomalies defined from ERA-5 reanalysis and HadISST, and multimodel mean regression coefficients from (center) 28 CMIP5 models and (right) 34 CMIP6 models based on 200 years of preindustrial control variability. The plotted regression coefficients are for a one standard deviation anomaly (σ) in each cloud controlling factor (as calculated from observations) at each grid point. Stippling in the left column indicates regions where the regression coefficients are 95% statistically significant via a standard Student's t test (for fine stippling) and the Wilks (2016) methodology (for bold stippling). Note that the color scale is different in (a)–(c).

(Fig. 4). Overall, models capture the spatial pattern of the observed sensitivities correctly (Figs. 1b,c), but generally overestimate the sensitivity of midlatitude clouds to vertical velocity perturbations (Norris and Weaver 2001; GM16; Kelleher and Grise 2019). Notably, the bias over midlatitude oceans has significantly improved in CMIP6 models, but the models remain biased compared to observations (Figs. 2a–c and 3a). Models' longwave CRE are also overly sensitive to vertical velocity perturbations, but as for shortwave CRE, there are significant reductions in these biases at midlatitudes in CMIP6 models (Figs. S2–S4).

The observed sensitivity of shortwave CRE to EIS variations is positive in tropical deep convective regions and negative in subtropical low cloud regions and in midlatitudes (Fig. 1d; see also Fig. 6b of GM16). The sensitivities switch sign near where the climatological value of EIS is 2 K (GM16). In the deep tropics where a boundary layer temperature inversion is weak or absent, the positive sensitivity indicates that enhanced boundary layer stability is associated with decreased cloud reflection (positive shortwave CRE anomalies), as enhanced low-level stability inhibits high-topped free-tropospheric cloud formation within these deep convective regimes (Fig. 4c). In the subtropical low cloud regions and in midlatitudes where the climatological inversion strength exceeds 2 K, the negative sensitivity indicates that enhanced boundary layer stability is associated with increased cloud reflection (negative shortwave CRE anomalies), consistent with the well-documented relationship between EIS and low cloud cover in these regions (Fig. 4d; Wood and Bretherton 2006; Myers and Norris 2013; GM16). Models capture the spatial pattern of the observed sensitivities correctly (Figs. 1e,f), but generally underestimate the magnitude of the negative sensitivity in the subtropics (Qu et al. 2015) and midlatitudes (GM16; Zelinka et al. 2018; Kelleher and Grise 2019). The model biases are largest in the subtropics and Northern Hemisphere (NH) midlatitudes (Figs. 2d,e), and the biases have not notably improved from CMIP5 to CMIP6 models (Figs. 2f and 3b).

The observed sensitivity of shortwave CRE to variations in near-surface temperature advection is generally positive and is most robust in subtropical low cloud regions and over the Southern Ocean (Fig. 1g). In these regions, the positive sensitivity indicates that near-surface cold advection is associated with increased cloud reflection (negative shortwave CRE anomalies), as the flow of cold air over relatively warmer water promotes the enhancement of turbulent surface fluxes and the development

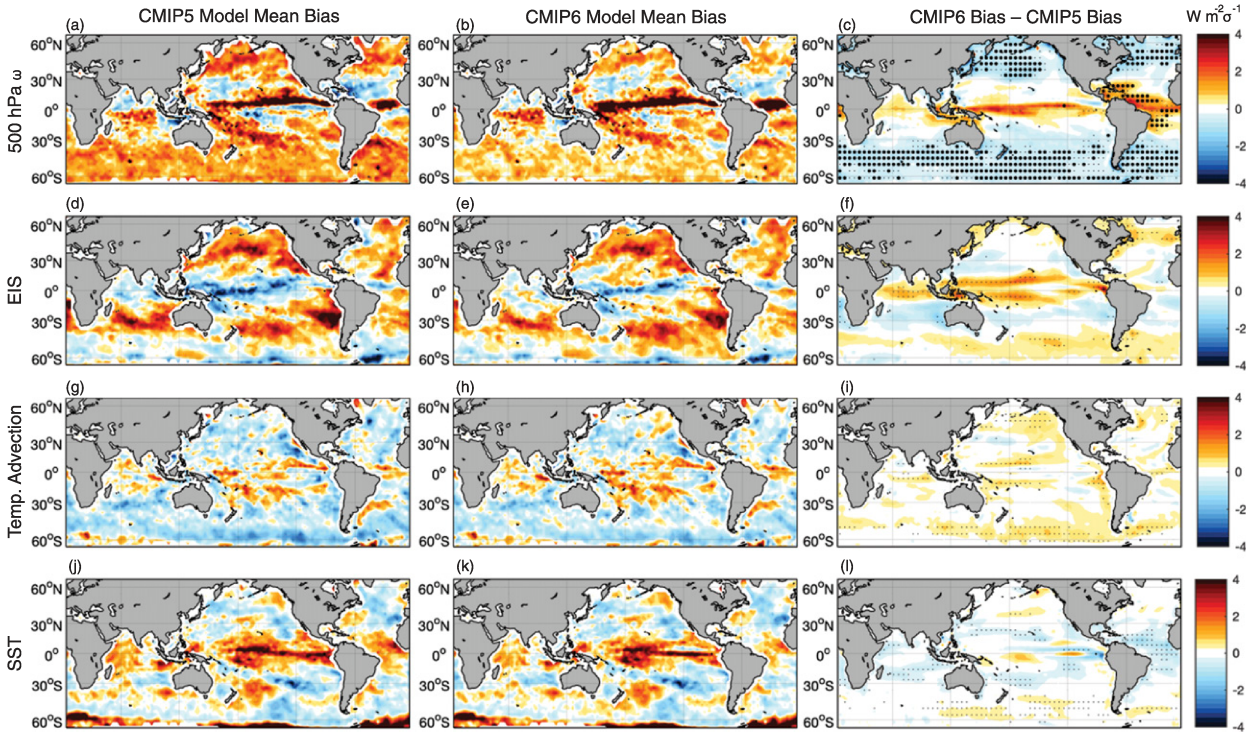

FIG. 2. Differences between the regression coefficients shown in Fig. 1: (left) CMIP5 multimodel mean − observations, (center) CMIP6 multimodel mean − observations, and (right) CMIP6 multimodel mean − CMIP5 multimodel mean. Stippling in the right column indicates regions where the difference between the multimodel means of CMIP5 and CMIP6 models is 95% statistically significant via a standard Student's *t* test (fine stippling) and the Wilks (2016) methodology (bold stippling).

of low cloud cover (Fig. 4f; Seethala et al. 2015; Miyamoto et al. 2018). Over midlatitude oceans, near-surface warm advection is also associated with increased high-topped free-tropospheric cloud fraction (Fig. 4e), reflecting the well-known relationship between mid-to-high-topped cloud cover and warm advection in midlatitude cyclones (e.g., Lau and Crane 1995; Norris and Iacobellis 2005), as would be expected from quasigeostrophic theory. The relationship between warm advection and free-tropospheric cloud fraction may also reflect the effects of moisture advection (Field and Wood 2007; McCoy et al. 2020). Over NH midlatitude oceans, the effects of warm and cold advection on cloud cover appear to largely compensate, resulting in a weak overall relationship between variations in shortwave CRE and near-surface temperature advection. Over the Southern Ocean, however, the cold advection (low cloud) effect dominates, resulting in the observed positive sensitivity of shortwave CRE to variations in near-surface temperature advection there. Models generally underestimate the area of the subtropics and midlatitudes characterized by a positive relationship between temperature advection and shortwave CRE (Figs. 1h,i). While CMIP6 models on average have slightly improved with respect to CMIP5 models over midlatitude oceans (Figs. 2g–i), approximately 75% of the models still underestimate the observed sensitivity over the Southern Ocean (Fig. 3c).

Finally, the observed sensitivity of shortwave CRE to SST variations is positive over most of the world's oceans, with the largest signatures occurring in the subtropics (Fig. 1j). Consistent with previous studies (e.g., Myers and Norris 2015, 2016), the positive sensitivity indicates that cold SST anomalies are associated with increased low cloud fraction (Fig. 4h) and thus increased cloud reflection (negative shortwave CRE anomalies) in these regions. Two exceptions are in deep convective regions along the ITCZ, where warmer SSTs are associated with increased high-topped free-tropospheric cloud fraction (Fig. 4g), and in high-latitude regions with variable sea ice cover, where variations in the underlying clear-sky surface albedo with SST complicate the interpretation of shortwave CRE. Models capture the spatial pattern of the observed sensitivities correctly (Figs. 1k,l), although they generally underestimate the observed magnitude (Figs. 2j,k). One exception is at SH midlatitudes, where the models on average slightly overestimate the observed positive shortwave CRE sensitivity to SST variations (Fig. 3d). There has been little improvement of these biases from CMIP5 to CMIP6 models (Figs. 2l and 3d), with CMIP6 models showing slightly greater increases in shortwave CRE with increases in SST at SH midlatitudes [consistent with the results of Zelinka et al. (2020)].

In summary, persistent biases in the sensitivity of midlatitude shortwave CRE to large-scale environmental cloud controlling factors remain in CMIP6 models. Midlatitude shortwave CRE are too sensitive to variations in vertical velocity and not sensitive enough to variations in EIS and near-surface temperature advection (Figs. 1–3). Biases in the sensitivity of midlatitude shortwave CRE to variations in SST vary by region (Figs. 2j,k).

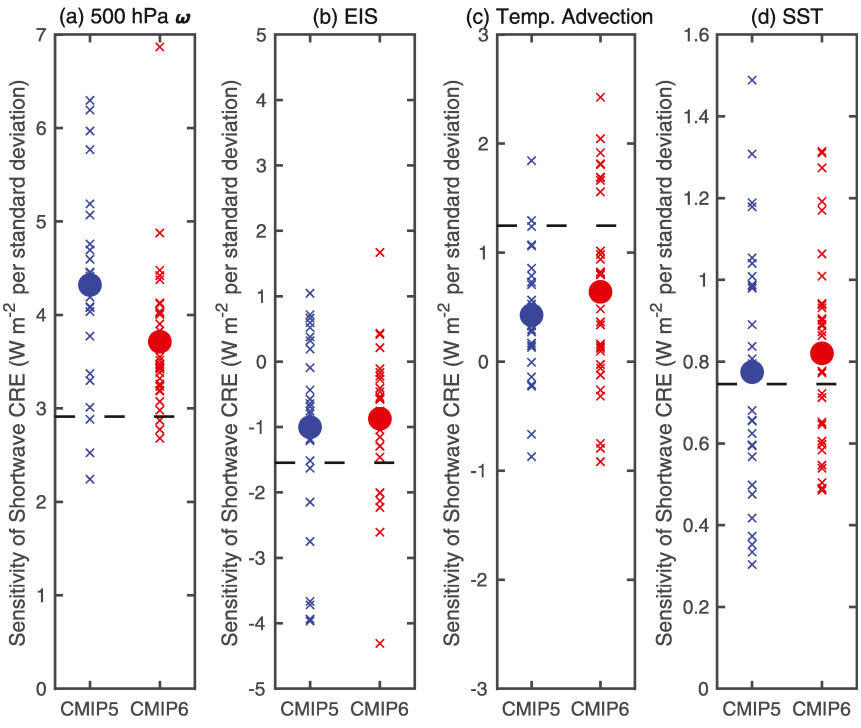

FIG. 3. Regression coefficients shown in Fig. 1 averaged over ocean regions between 30° and 60°S. Dashed horizontal lines show the observational values, blue (CMIP5) and red (CMIP6) crosses show values from individual CMIP models, and large dots show the multimodel-mean values.

Relative to observations, the most notable improvements from CMIP5 to CMIP6 models have been in the vertical velocity and near-surface temperature advection sensitivities (Figs. 2c,i and 3a,c).

Now, having reviewed the global sensitivities of shortwave CRE to the four midlatitude cloud controlling factors in observations and models, we explore two applications of these results in the remainder of the paper. First, in section 4, we explore how the midlatitude cloud controlling factor sensitivities are relevant in explaining the diverse cloud radiative effects in models associated with meridional shifts in the SH midlatitude jet stream. Then, in section 5, we explore whether the midlatitude cloud controlling factor sensitivities are linked to the spread in ECS across models.

4. Jet-CRE and midlatitude cloud controlling factors

As discussed in the introduction, many CMIP5 models simulate a net shortwave warming effect when the SH midlatitude jet stream shifts poleward, but such an effect is not present in observations (GP14). In this section, we examine whether the improvements in the sensitivity of CRE to the midlatitude cloud controlling factors in CMIP6 models (as detailed in section 3) have led to a better representation of the CRE anomalies associated with a SH midlatitude jet shift. Following GP14, in Fig. 5, we show the regressions of shortwave CRE anomalies onto anomalies in the latitude of the SH midlatitude jet during the December–February (DJF) season; qualitatively similar results are found if the regressions are performed over all months, as opposed to just DJF. Corresponding results for longwave CRE are shown in Fig. S5. The spatial pattern of longwave CRE anomalies associated with a poleward shift in the SH midlatitude jet is consistent with a simple poleward shift of storm-track clouds and closely mirrors that of high-topped cloud cover (Grise et al. 2013; GM16). Observations and models much more closely agree on the longwave CRE anomalies associated with a poleward SH jet shift (Fig. S5; GP14; GM16), so for the remainder of this section we focus our discussion on the shortwave CRE anomalies shown in Fig. 5, which vary more widely between observations and models.

The observed pattern of shortwave CRE anomalies associated with a 1° poleward shift in the SH midlatitude jet is shown in Fig. 5a. The results are nearly identical to those shown in Fig. 4 of GP14, except that here we use an updated version of the CERES EBAF dataset and use the TropD code package to calculate jet latitude instead of the method from Barnes and Polvani (2013). As found by GP14, the observed shortwave CRE anomalies are noisy and widely vary across the Southern Ocean. Variations in the underlying clear-sky surface albedo due to changes in sea ice cover complicate the interpretation of shortwave CRE in regions adjacent to the Antarctic coastline, and the relatively short observational record may also contribute to the noisiness of the spatial pattern. Nevertheless, we have confidence in the pattern of shortwave CRE anomalies

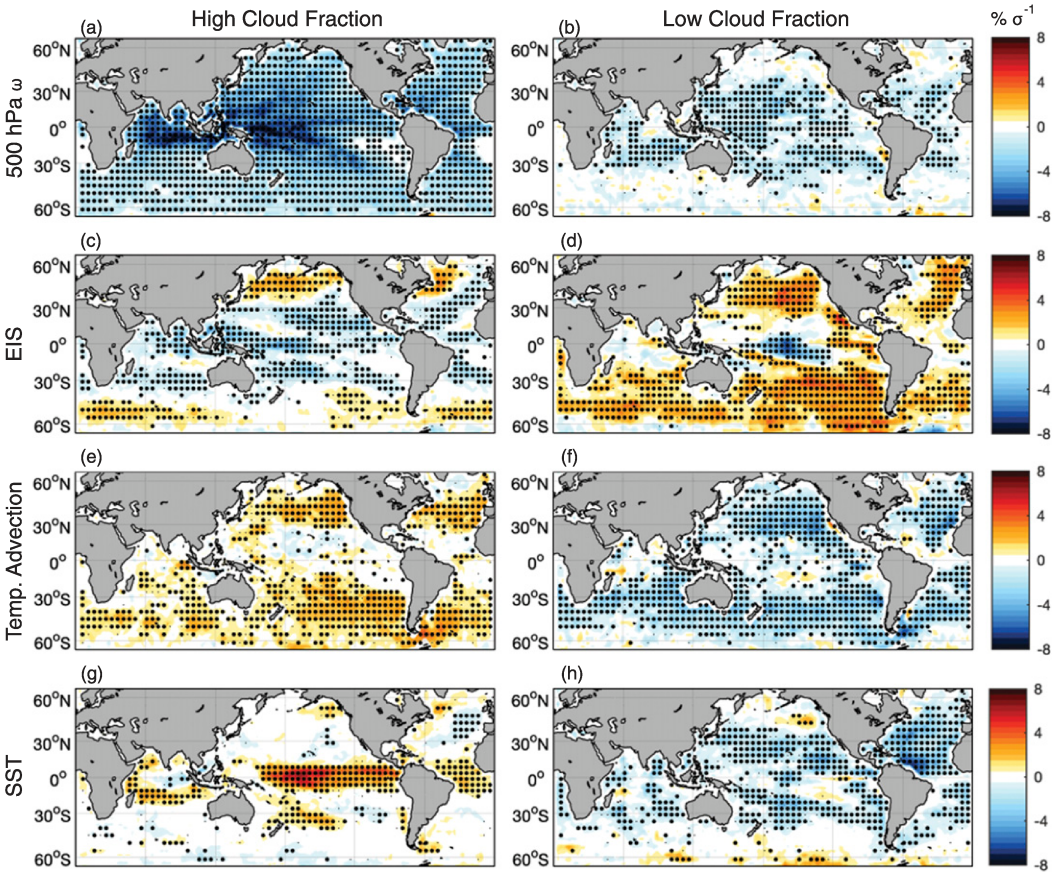

FIG. 4. As in the left column of Fig. 1, but for regressions of monthly ISCCP high cloud fraction (cloud-top pressure < 440 hPa) and low cloud fraction (cloud-top pressure > 680 hPa) anomalies onto monthly anomalies in four cloud controlling factors over the period July 1983–June 2008. Low cloud fraction anomalies are calculated using the random overlap assumption [Eq. (1)].

shown in Fig. 5a, as similar patterns of shortwave CRE anomalies can be derived from hundreds of years of preindustrial control variability in certain climate models (see Fig. 3b of GP14).

Overall, Fig. 5a demonstrates that the observed shortwave CRE anomalies associated with a poleward shift in the SH midlatitude jet do not show a coherent zonally symmetric warming at midlatitudes as would be expected from a simple poleward shift of the storm-track clouds. In fact, the average of the shortwave CRE anomalies over SH midlatitudes (30°–60°S)—what GP14 term the "jet-CRE index"—is negative ($-0.39\,\mathrm{W\,m^{-2}}$). In contrast to observations, CMIP5 models on average show zonally symmetric positive shortwave CRE anomalies at SH midlatitudes when the jet shifts poleward (Fig. 5b; GP14; GM16). This bias has been slightly reduced in CMIP6 models, but largely remains (Fig. 5c).

To assess the behavior of individual models, Fig. 5d plots the jet-CRE index (i.e., the values in Figs. 5b and 5c averaged over 30°–60°S) for all models examined in this study. The values of the jet-CRE index for each model are also listed in Tables 1 and 2. The values of the jet-CRE indices for CMIP5 models are very similar but not identical to those given by GP14 because, in this study, we use a slightly different method to calculate jet latitude and calculate regression coefficients using monthly-mean anomalies (as opposed to seasonal-mean anomalies in GP14). GP14 referred to models with positive jet-CRE indices as type I, indicating that they had a net shortwave warming effect at SH midlatitudes associated with a poleward jet shift. Models with negative jet-CRE indices (i.e., those that more closely resembled observations) were termed type II. Of the models we examine here, 19 of the 28 CMIP5 models are type I, and 19 of the 34 CMIP6 models are type I (Fig. 5d). While on average CMIP6 models have slightly improved relative to observations, the type I bias still remains in many CMIP6 models.

Can the cloud controlling factor framework be used to explain this persistent model bias? First, in the left column of Fig. 6, we review how each of the four midlatitude cloud controlling factors change with a 1° poleward shift in the SH midlatitude jet. The results shown in the left column of Fig. 6 are from observations; qualitatively similar results are found in both CMIP5 and CMIP6 models (Fig. S6). The vertical velocity anomalies associated with a poleward SH jet shift are consistent with a poleward shift of the midlatitude storm tracks, with

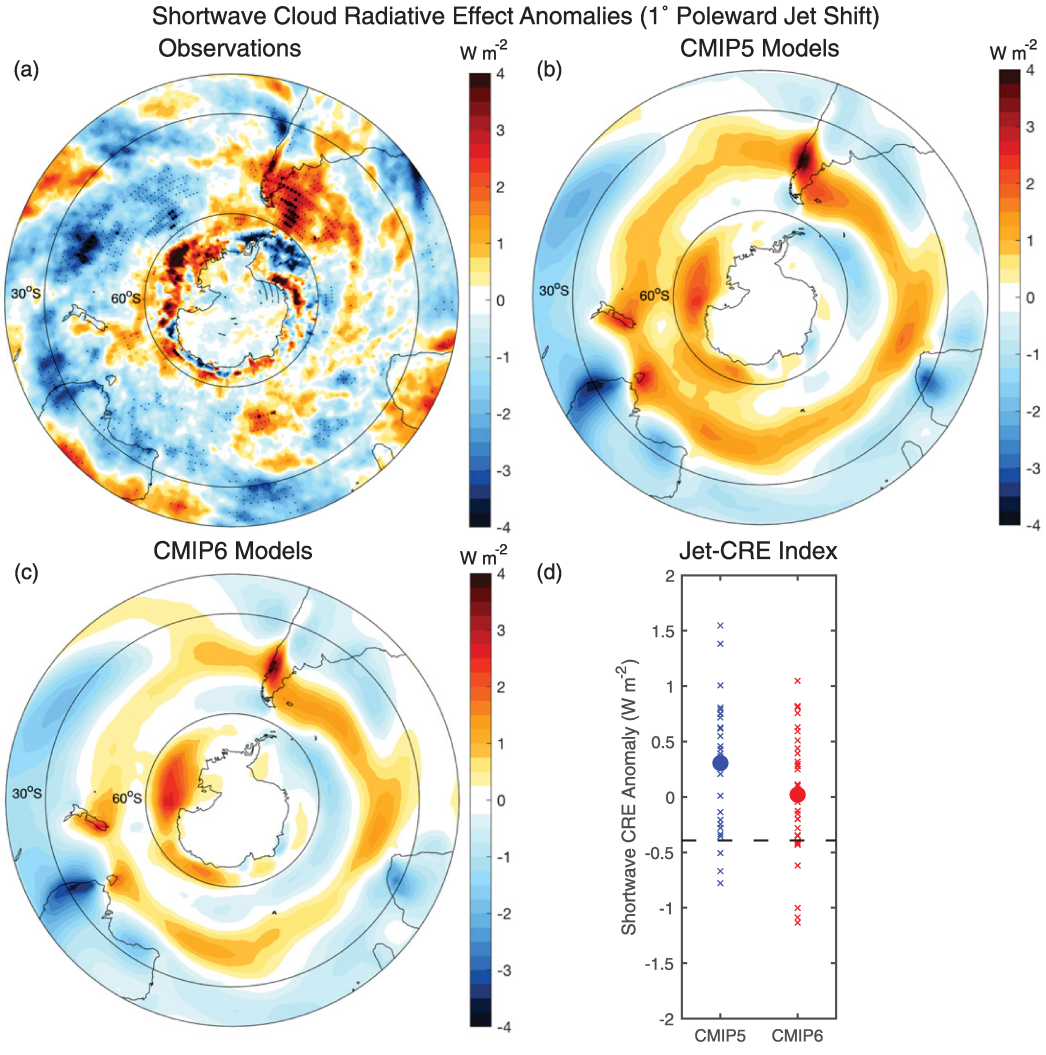

FIG. 5. Regressions of monthly December–February shortwave CRE anomalies onto anomalies in the latitude of the SH midlatitude eddy-driven jet. Magnitudes shown correspond to a 1° latitude poleward shift in the jet. Results are shown for (a) 2001–18 CERES shortwave CRE anomalies regressed on the jet latitude defined from ERA-5 reanalysis and (b),(c) multimodel mean regression coefficients from 28 CMIP5 models and 34 CMIP6 models based on 200 years of preindustrial control variability. Stippling in (a) indicates regions where the regression coefficients are 95% statistically significant via a standard Student's t test (fine stippling) and the Wilks (2016) methodology (bold stippling). (d) The magnitudes of the regression coefficients shown in (a)–(c) averaged over 30°–60°S, where the dashed black line is the observed value, blue (CMIP5) and red (CMIP6) crosses show values from individual CMIP models, and large dots show the multimodel-mean values.

anomalous subsidence (positive ω_{500} anomalies) near the mean jet position (51°S) and anomalous ascent (negative ω_{500} anomalies) poleward of there (Fig. 6a; see also GM16). The EIS anomalies associated with a poleward SH jet shift closely mirror the vertical velocity anomalies, as enhanced subsidence promotes a warming and drying of the free troposphere and consequently a strengthening of the boundary layer temperature inversion (Fig. 6d; see also GM16). The near-surface temperature advection anomalies associated with a poleward SH jet shift are noisy, with the exception of a region of strong warm advection associated with the major SH storm-track cyclogenesis region off the east coast of South America (Fig. 6g). Finally, the SST anomalies associated with a poleward SH jet shift reflect changes in Ekman transport and surface turbulent fluxes induced by the poleward shift in westerly wind stress (Fig. 6j; Sen Gupta and England 2006; Ciasto and Thompson 2008).

Now, to assess the contribution of each cloud controlling factor to the shortwave CRE anomalies associated with a 1° poleward shift of the SH midlatitude jet (as shown in Fig. 5), we multiply the sensitivity of shortwave CRE to each cloud controlling factor (as shown in Fig. 1) by the change in cloud controlling factor for a 1° poleward shift of the SH midlatitude jet (as shown in the left column of Fig. 6). Results for the

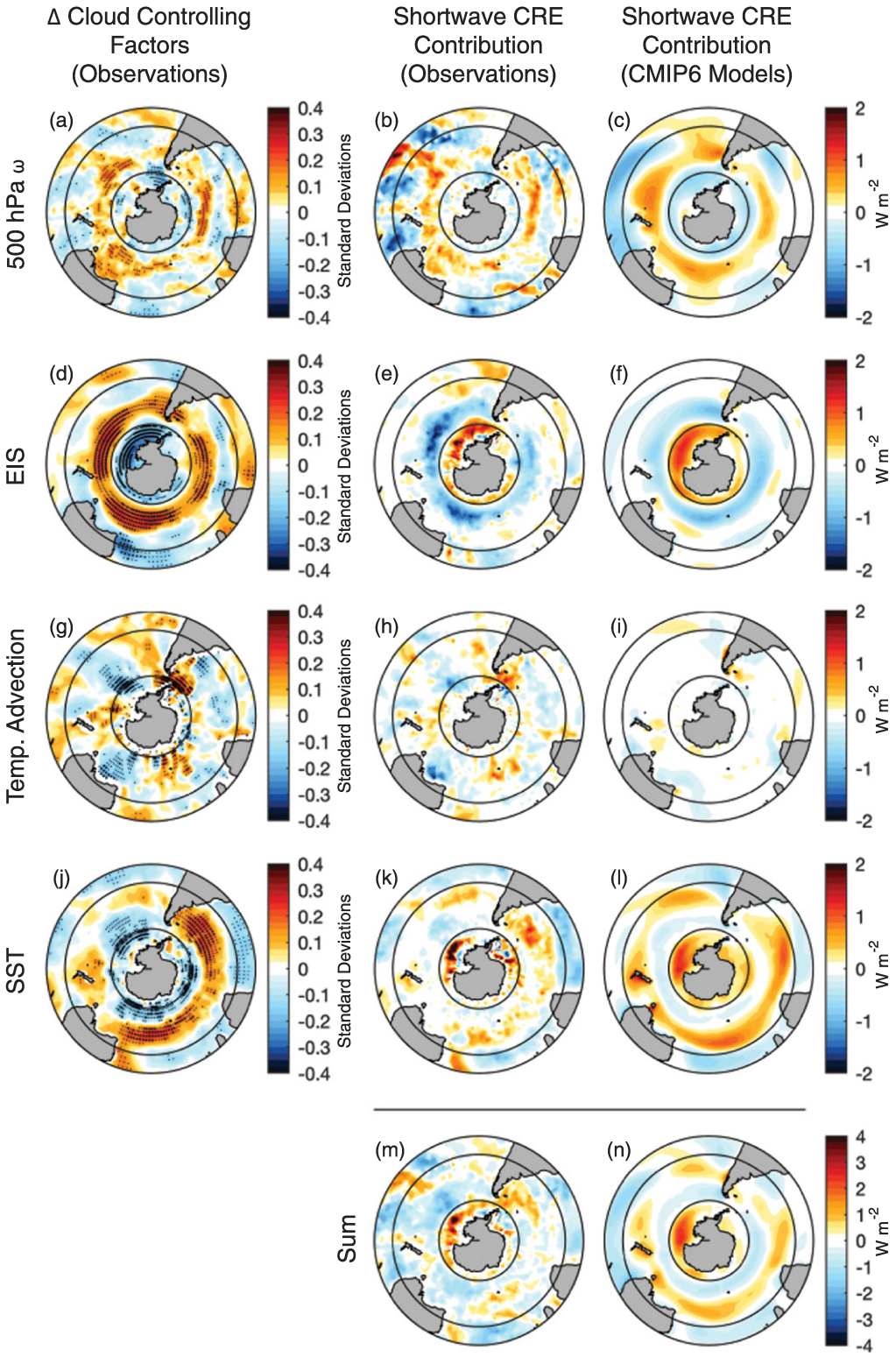

FIG. 6. (left) Regressions of observed monthly December–February anomalies in each of the four cloud controlling factors onto anomalies in the latitude of the SH midlatitude eddy-driven jet. Magnitudes shown correspond to a 1° latitude poleward shift in the jet. The regression coefficients are plotted in units of standard deviations at each grid point. Stippling indicates regions where the regression coefficients are 95% statistically significant via a standard Student's *t* test (fine stippling) and the Wilks (2016) methodology (bold stippling). (center) Contribution of each cloud controlling factor to the observed shortwave CRE signature associated with a 1° latitude poleward shift in the jet (as shown in Fig. 5a), as defined from Eq. (3). (right) As in the center column, but for the CMIP6 multimodel mean (as shown in Fig. 5c). (m),(n) The sum of the upper four panels in their respective columns.

observations are shown in the center column of Fig. 6, and results for CMIP6 models are shown in the right column of Fig. 6. Results for CMIP5 models are nearly identical to CMIP6 models and are not shown for brevity. Note that the summation of the CRE anomalies associated with each cloud controlling factor (Figs. 6m,n) well reproduces the spatial pattern of CRE anomalies shown in Fig. 5 (although the magnitudes are underestimated), providing evidence of the utility of the multiple linear regression model [Eq. (3)].

Figure 6 reveals that the shortwave CRE anomalies associated with a poleward shift of the SH midlatitude jet reflect the competing contribution of three cloud controlling factors: vertical velocity, EIS, and SST. Anomalous subsidence over the Southern Ocean is associated with positive shortwave CRE anomalies (Figs. 6b,c), consistent with a poleward shift of high-topped storm-track clouds (see Fig. 1a of GM16). Increases in EIS over the Southern Ocean are associated with negative shortwave CRE anomalies (Figs. 6e,f), consistent with an increase in low cloud fraction on the equatorward flank of the jet in the region vacated by storm-track clouds (see Fig. 1b of GM16). Increases in SST on the equatorward side of the region of anomalous subsidence are associated with positive shortwave CRE anomalies (Figs. 6k,l), consistent with the relationship between positive SST anomalies and reduced low cloud fraction in this latitude band (Fig. 4h). Near-surface temperature advection plays a minimal role in the shortwave CRE anomalies associated with a poleward shift of the SH midlatitude jet (Figs. 6h,i).

The model biases in the shortwave CRE anomalies associated with a poleward shift in the SH midlatitude jet arise for three reasons. First, the positive vertical velocity contribution is too large (Fig. 6c), mainly because of the oversensitivity of midlatitude CRE to vertical velocity anomalies (Figs. 1–3). This is a systematic problem across almost all models (Fig. 3a), but it does not explain a large fraction of the variance in the intermodel spread in the jet-CRE index (not shown). Second, the negative EIS contribution is too weak (Fig. 6f), largely because of the underestimated sensitivity of midlatitude shortwave CRE to EIS (Fig. 3b). Unlike vertical velocity, the varying EIS sensitivity across models explains a substantial fraction of the intermodel variance (55% in CMIP5 models, 44% in CMIP6 models) in the jet-CRE index (Fig. 7a). From Fig. 7a, it appears that one reason that the majority of CMIP5 and CMIP6 models display type I behavior (jet-CRE index > 0) is that they underestimate EIS sensitivity at SH midlatitudes. Because the models' sensitivity of SH midlatitude shortwave CRE to EIS variations has not notably improved from CMIP5 to CMIP6 models (Fig. 3b), the models' cloud radiative response to a poleward jet shift also remains biased on average in CMIP6 models (Fig. 5), despite other improvements in model cloud parameterizations. We note that the correlations between the jet-CRE index and the sensitivity of models' shortwave CRE to cloud controlling factors other than EIS are not nearly as large or as consistent between CMIP5 and CMIP6 models (not shown).

The third and final reason for the model bias in the shortwave CRE anomalies associated with a poleward shift in the SH midlatitude jet is that the positive SST contribution is too large (Fig. 6l). Unlike the vertical velocity and EIS contributions, this does not result from biases in the model shortwave CRE sensitivity to SST perturbations (Fig. 3d), but rather from an overestimation of the SST anomalies associated with a poleward jet shift (see Fig. S6). The exaggerated magnitude of SST anomalies associated with a SH midlatitude jet shift is a well-documented problem in CMIP models (e.g., Karpechko et al. 2009; Screen et al. 2010). Like the varying EIS sensitivity across models, the varying magnitudes of the SST anomalies associated with a poleward SH jet shift explain a sizeable fraction of the intermodel variance (32%) in the jet-CRE index (Fig. 7b). So, Fig. 7b reveals that another reason that the majority of CMIP5 and CMIP6 models display type I behavior (jet-CRE index > 0) is that they systematically overestimate the SST anomalies at SH midlatitudes, and this bias has also not notably improved from CMIP5 to CMIP6 models. We note that the correlations between the jet-CRE index and the magnitude of the responses of the other cloud controlling factors (other than SST) to a jet shift are not nearly as large or as consistent between CMIP5 and CMIP6 models (not shown).

In CMIP5 models, GP14 documented a significant correlation ($|r| = 0.75$) between the jet-CRE index and the climatological magnitude of shortwave CRE over the Southern Ocean. GP14 suggested that there was a trade-off in models between a proper representation of the climatology and a proper representation of the cloud processes associated with a jet shift. Models with more realistic climatological magnitudes of shortwave CRE over the Southern Ocean were found to be type I models, whereas models with more realistic values of jet-CRE were found to underestimate the observed climatological magnitude of shortwave CRE over the Southern Ocean. In Fig. 7c, we reproduce this correlation ($|r| = 0.66$) using the subset of CMIP5 models examined in this study, but we find that this relationship is less apparent in CMIP6 models ($|r| = 0.37$).

What is the impact of the model bias in the shortwave CRE anomalies associated with a SH midlatitude jet shift? Because the SH jet shifts robustly poleward in response to increasing greenhouse gases (e.g., Barnes and Polvani 2013; Vallis et al. 2015; Grise and Polvani 2016), one might suspect that the CRE associated with a SH midlatitude jet shift may directly feed back on the global-mean surface temperature response (e.g., Boucher et al. 2013). However, as shown in Fig. 7d, the jet-CRE index is poorly correlated with ECS in both CMIP5 and CMIP6 models. This result is consistent with previous studies (e.g., Kay et al. 2014; Ceppi and Hartmann 2015; Wall and Hartmann 2015), which have concluded that thermodynamic processes are of much greater importance for SH midlatitude cloud feedbacks.

Instead, the cloud radiative anomalies associated with midlatitude jet shifts may be more relevant for the transient surface temperature response to increasing greenhouse gases. Figure 8 shows the correlations of the jet-CRE index with the zonal-mean surface temperature response to abrupt $4xCO_2$ forcing in both CMIP5 and CMIP6 models. We focus only on the correlations that are robust in both CMIP5 and CMIP6 models, as it is less likely that these correlations simply occur by chance. While the correlations in Fig. 8 differ substantially between CMIP5 and CMIP6 models, one common feature is a positive correlation around 40°S within the first decade after CO_2

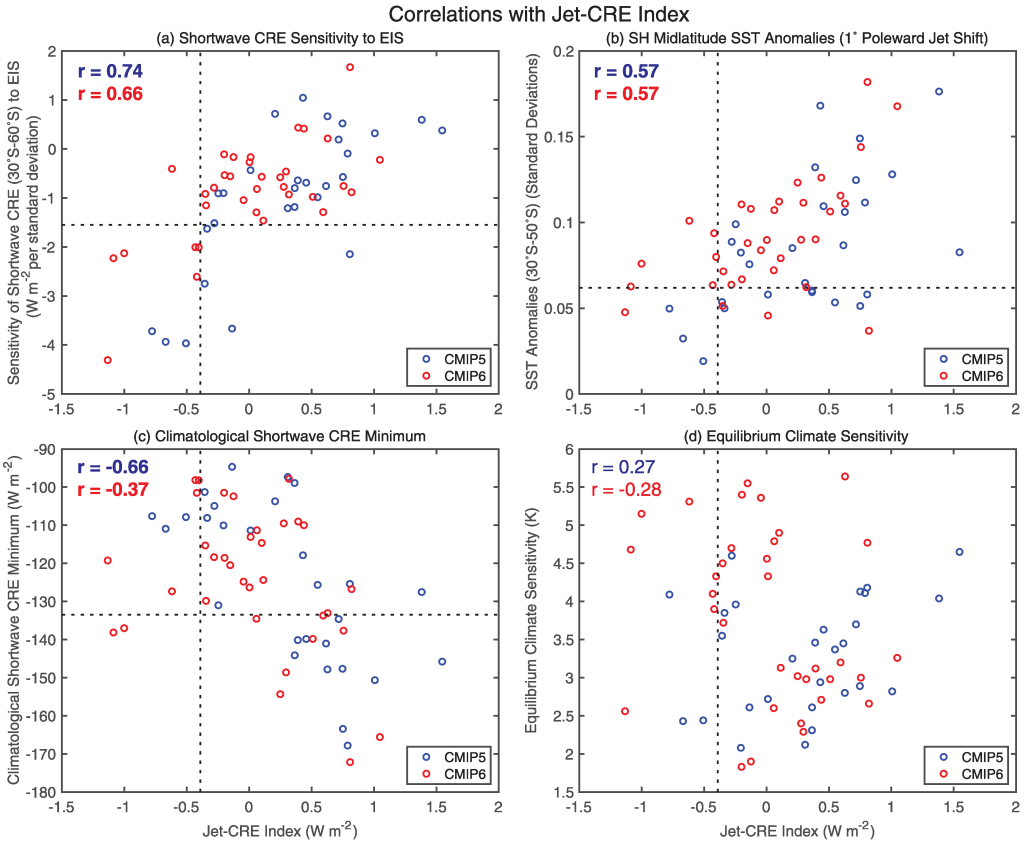

FIG. 7. Scatterplots of jet-CRE index (as shown in Fig. 5d) vs (a) the sensitivity of shortwave CRE anomalies to EIS perturbations at SH midlatitudes (as shown in Fig. 3b), (b) SST anomalies (averaged over 30°–50°S) associated with a 1° poleward shift in the SH midlatitude jet (as shown in Fig. 6j and Figs. S6j–l), (c) the climatological minimum value of zonal-mean shortwave CRE at SH midlatitudes during DJF, and (d) equilibrium climate sensitivity. Observed values are denoted by the black dashed lines. Correlation coefficients that are 95% statistically significant via Student's *t* test are listed in bold type.

quadrupling. As discussed by Grise and Polvani (2017) and Ceppi et al. (2018), the poleward shift of the SH midlatitude jet in response to abrupt 4xCO_2 forcing occurs very rapidly (within the first 5–10 years), much faster than the response of the global-mean surface temperature. As a result, the cloud radiative anomalies associated with the jet shift appear first before thermodynamic feedbacks can dominate, resulting in an initially larger surface temperature warming near 40°S in type I models within the first decade after CO_2 quadrupling (Fig. 8; see also discussion in GP14). Thus, while cloud radiative anomalies associated with midlatitude jet shifts are not of first-order importance to the equilibrium surface temperature response to increasing greenhouse gases (Fig. 7d), they likely play a greater role in the transient regional temperature response at midlatitudes.

In summary, both CMIP5 and CMIP6 models on average simulate positive shortwave CRE anomalies at SH midlatitudes in response to a poleward shift in the SH midlatitude jet, an effect that is not present in observations (Fig. 5). This bias is closely linked to the models' overestimated sensitivity of shortwave CRE to vertical velocity variations (Figs. 3a and 6c), underestimated sensitivity of shortwave CRE to EIS variations (Figs. 3b, 6f, and 7a), and overestimated SST anomalies associated with SH jet shifts (Figs. 6l and 7b). All three of these problems remain persistent from CMIP5 to CMIP6 models, resulting in little improvement in the magnitude of the shortwave CRE anomalies associated with SH jet shifts from CMIP5 to CMIP6 models (Fig. 5d). While the cloud radiative anomalies associated with midlatitude jet shifts are not directly relevant for ECS (Fig. 7d), they may still impact transient regional surface temperature responses at midlatitudes (Fig. 8). In the next section, we turn our attention to those midlatitude cloud processes that are more closely linked to ECS.

5. Equilibrium climate sensitivity and midlatitude cloud controlling factors

In this section, we briefly explore the relationship between the sensitivities of CRE to the four midlatitude cloud controlling factors in CMIP models (as detailed in section 3) with ECS. In other words, we seek to understand whether models with better representations of the observed CRE sensitivities

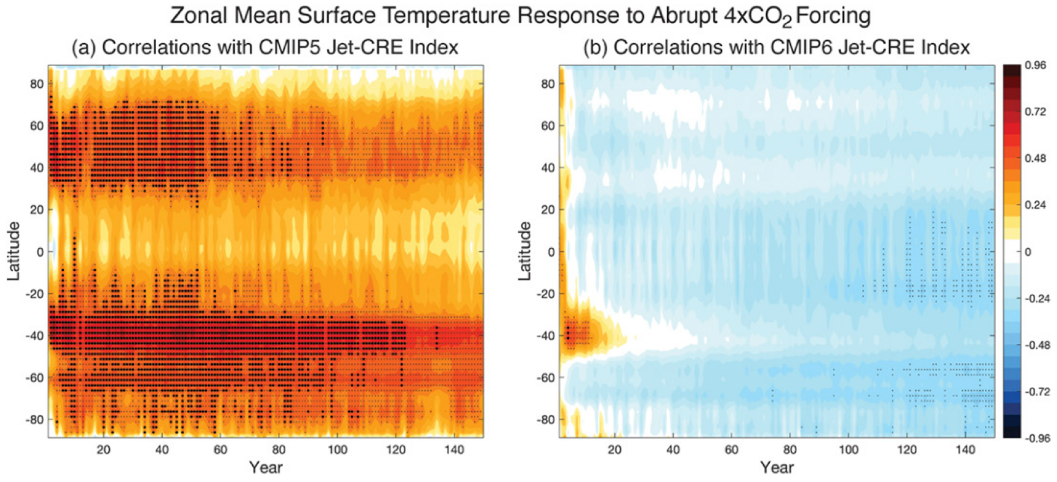

FIG. 8. Correlations between the jet-CRE index (as shown in Fig. 5d) and the zonal-mean surface temperature response to abrupt 4xCO_2 forcing for (a) CMIP5 models and (b) CMIP6 models. The response to abrupt 4xCO_2 forcing is defined as the difference between the abrupt4xCO_2 scenario and the preindustrial control climatology. Stippling indicates regions where the correlation coefficients are 95% statistically significant via a standard Student's t test (fine stippling) and the Wilks (2016) methodology (bold stippling).

to the cloud controlling factors (Fig. 1, left column) necessarily have higher or lower values of ECS. Figure 9 displays the correlations between the ECS of each model and the sensitivity of its shortwave CRE to variations in the four midlatitude cloud controlling factors (as shown in Fig. 1). Correlations between the ECS of each model and the sensitivity of its net CRE (i.e., the sum of the shortwave and longwave components) to variations in the cloud controlling factors are dominated by the shortwave component, so we do not consider the longwave component here.

Figure 9 reveals that there are few consistent correlations between ECS and the cloud controlling factor sensitivities that are significant (via a standard Student's t test) across both CMIP5 and CMIP6 models, and none of the correlations are significant according to the stricter Wilks (2016) methodology. In interpreting Fig. 9, we focus again on only those relationships that are robust across both the CMIP5 and CMIP6 generations of models, as it is less likely that these correlations simply arise by chance. Many previous studies have highlighted the important role of subtropical marine low cloud processes in governing the intermodel spread in ECS (e.g., Bony and Dufresne 2005; Soden and Vecchi 2011; Vial et al. 2013), so unsurprisingly, there are some significant correlations between the models' ECS and their shortwave CRE sensitivities to EIS and SST perturbations in subtropical low cloud regions. Alternatively, Zelinka et al. (2020) recently concluded that, on average, CMIP6 models have larger values of ECS than CMIP5 models because of changes in their low cloud sensitivity to SST perturbations at SH midlatitudes. Consistent with this argument, Fig. 9h shows that CMIP6 models with larger increases in shortwave CRE for a given SST increase at SH midlatitudes generally have larger values of ECS, but such a relationship is not present in CMIP5 models (Fig. 9g). Instead, we find here that one of the significant correlations that is most consistent across both CMIP5 and CMIP6 models is between models' ECS and their shortwave CRE sensitivity to near-surface temperature advection perturbations near 40°S (Figs. 9e,f). This is explored further in Fig. 10. There are also some significant correlations between models' ECS and their shortwave CRE sensitivity to EIS perturbations between 45° and 60°S in both CMIP5 and CMIP6 models (Figs. 9c,d), but these correlations are largely driven by a few outlier models (not shown).

Figure 10a shows the scatterplot between the ECS of each model and its shortwave CRE sensitivity to near-surface temperature advection perturbations at 40°S (as shown in Fig. 3c, but for 40°S). Consistent with Figs. 9e and 9f, a significant positive correlation exists for both CMIP5 ($r = 0.38$) and CMIP6 ($r = 0.50$) models. The observed shortwave CRE sensitivity to near-surface temperature advection falls above the 80th percentile of model values (see also Fig. 3c for the 30°–60°S latitude band). All but one model with temperature advection sensitivities equal to or greater than observations have values of ECS greater than 3.25 K. In contrast, the majority of models with temperature advection sensitivities less than observations have values of ECS between 2 and 4.5 K.

Figure 10b now examines the correlations of the models' temperature advection sensitivities at 40°S (as plotted on the abscissa in Fig. 10a) with the zonal-mean surface temperature response to abrupt 4xCO_2 forcing at the same latitude. Recall that in Fig. 8 we showed that, in the decade after an abrupt quadrupling of atmospheric CO_2 concentrations, the zonal-mean surface temperature response at this latitude reflects the cloud radiative processes associated with a midlatitude jet shift, which are closely linked to models' shortwave CRE sensitivities to EIS perturbations (Fig. 7a). Here in Fig. 10b we show that, in the subsequent decades, the surface temperature response in this latitude band becomes more strongly controlled by the cloud radiative processes linked to models'

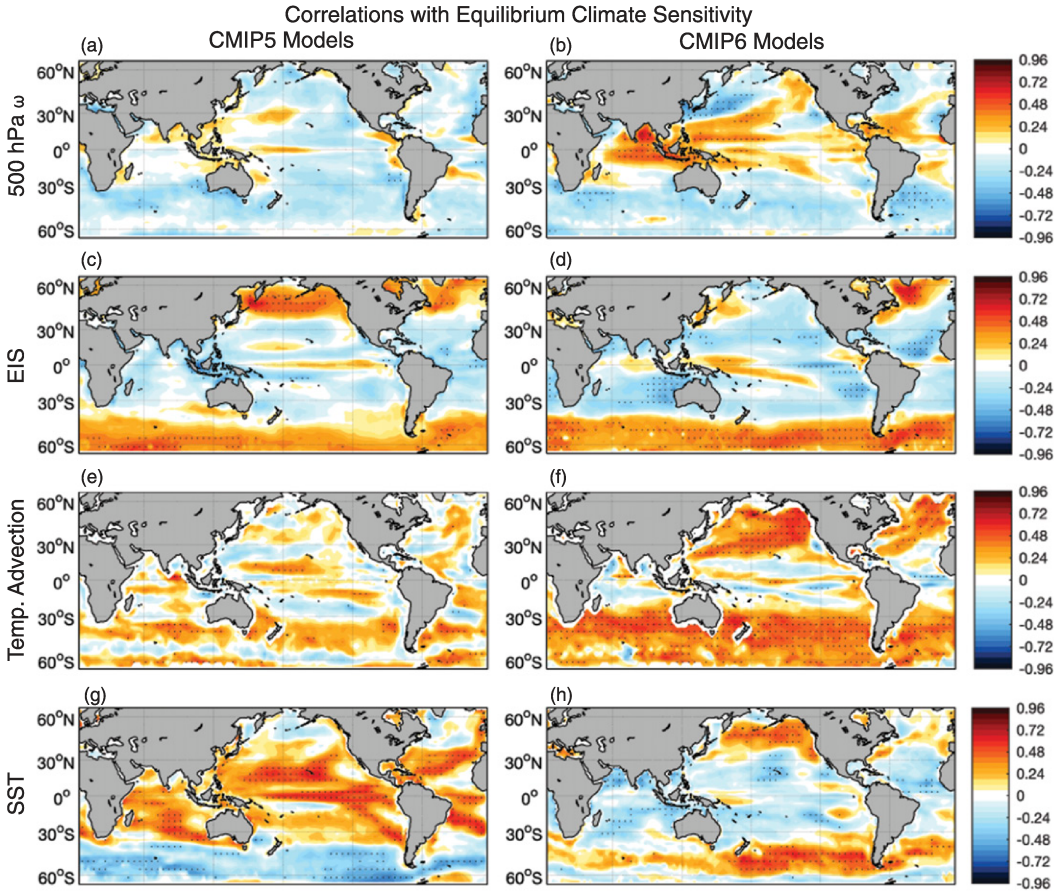

FIG. 9. Correlations between the equilibrium climate sensitivity and the sensitivities of shortwave CRE anomalies to four cloud-controlling factors (as shown in Fig. 1) across (left) 28 CMIP5 models and (right) 34 CMIP6 models. Stippling indicates regions where the correlation coefficients are 95% statistically significant via a standard Student's *t* test. No regions are statistically significant via the Wilks (2016) methodology.

shortwave CRE sensitivities to near-surface temperature advection perturbations. Thus, the observed sensitivity of shortwave CRE to EIS perturbations may help to constrain the transient surface temperature response to climate change near 40°S (Figs. 8 and 10c), whereas the observed sensitivity of shortwave CRE to near-surface temperature advection perturbations may help to constrain the longer-term surface temperature response at SH midlatitudes (and possibly also globally, as shown in Fig. 10a).

6. Conclusions

Cloud controlling factors serve as a useful framework for understanding the large-scale dynamic and thermodynamic processes responsible for driving observed cloud properties. In this study, we examine the fidelity of CMIP6 models in representing the observed sensitivities of midlatitude cloud radiative properties to variations in four cloud controlling factors (midtropospheric vertical velocity, EIS, near-surface temperature advection, and SST) and assess any improvements relative to CMIP5 models. Overall, we find that both CMIP5 and CMIP6 models on average overestimate the sensitivity of midlatitude CRE to perturbations in vertical velocity, and underestimate the sensitivity of midlatitude shortwave CRE to perturbations in EIS and near-surface temperature advection (Figs. 1–3). Biases in the sensitivity of midlatitude shortwave CRE to variations in SST vary by region (Figs. 2j,k). The sensitivity of midlatitude CRE to perturbations in vertical velocity—and to a lesser extent near-surface temperature advection—has improved in CMIP6 models relative to CMIP5 models (Figs. 2c,i).

The cloud controlling factor framework provides a useful perspective for understanding the CRE anomalies associated with a poleward shift in the SH midlatitude jet stream. When the SH jet shifts poleward, models on average simulate decreased reflection of shortwave radiation by clouds in the region equatorward of the jet, an effect not seen in observations (Fig. 5; GP14). This bias occurs in models for three reasons. First, when the jet shifts poleward, anomalous subsidence equatorward of the jet (Fig. 6a) promotes a decrease in high cloud cover, but because the CRE in models are too sensitive to vertical velocity perturbations (Fig. 3a), the associated

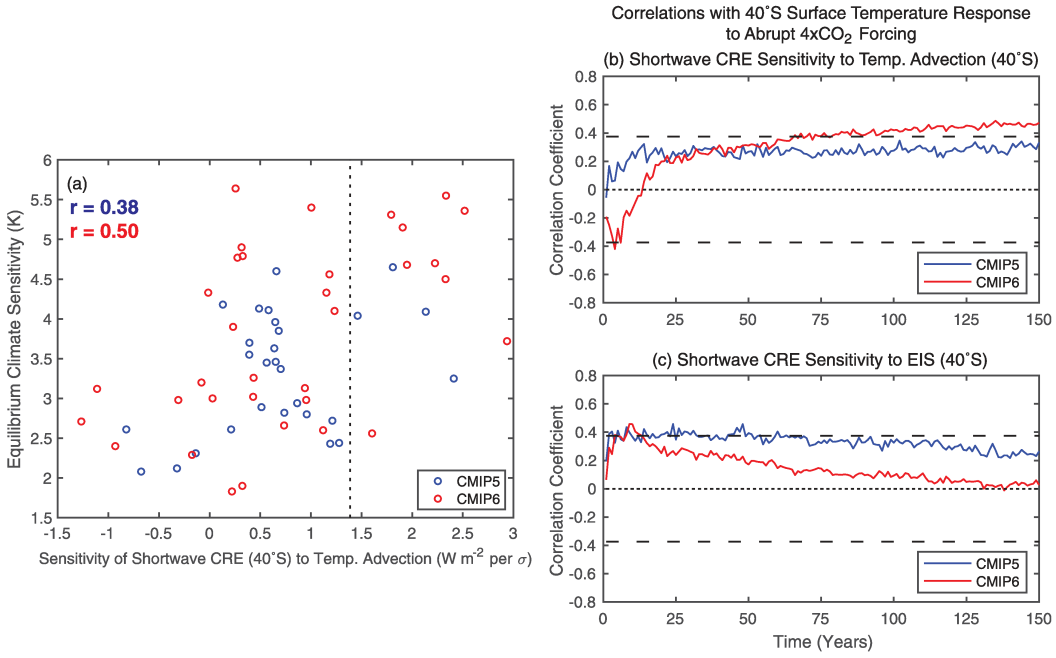

FIG. 10. (a) Scatterplot of the sensitivity of shortwave CRE anomalies to near-surface temperature advection perturbations at 40°S (as shown in Fig. 3c, but for 40°S) vs equilibrium climate sensitivity. The vertical black dashed line indicates the observed value of temperature advection sensitivity. Correlation coefficients that are 95% statistically significant via Student's t test are listed in bold type. (b) Correlations between the sensitivity of shortwave CRE anomalies to near-surface temperature advection perturbations at 40°S [as plotted on the abscissa in (a)] and the 40°S surface temperature response to abrupt $4xCO_2$ forcing. The horizontal black dashed lines indicate the magnitude above which the correlation coefficient is 95% statistically significant via Student's t test. (c) As in (b), but for correlations between the sensitivity of shortwave CRE anomalies to EIS perturbations at 40°S (as shown in Fig. 3b, but for 40°S) and the 40°S surface temperature response to abrupt $4xCO_2$ forcing.

reduction in the reflection of shortwave radiation by clouds is exaggerated in models compared to observations (Figs. 6b,c). Second, when the jet shifts poleward, EIS increases in the region equatorward of the jet vacated by the high-topped storm-track clouds (Fig. 6d), supporting an increase in low cloud cover in this region. However, because the shortwave CRE in models are not sensitive enough to EIS perturbations (Fig. 3b), the associated increase in the reflection of shortwave radiation by clouds is underestimated in models compared to observations (Figs. 6e,f). Finally, when the jet shifts poleward, SST increases in the region equatorward of the anomalous subsidence (Fig. 6j), promoting a decrease in low cloud cover in this region (Fig. 4h). Because models on average overestimate the SST anomalies associated with SH jet shifts (Fig. 7b; Karpechko et al. 2009; Screen et al. 2010), the associated reduction in the reflection of shortwave radiation by clouds is overestimated in models compared to observations (Figs. 6k,l).

All three of these biases are widespread among CMIP5 and CMIP6 models, so the cloud radiative anomalies associated with SH midlatitude jet shifts remain biased in many CMIP6 models (Fig. 5d), despite improved representation of other cloud processes relative to CMIP5 models. While these cloud radiative anomalies are not large enough to impact the global-mean surface temperature response to increasing atmospheric greenhouse gas concentrations (Fig. 7d), they play a role in determining the transient surface temperature response near 40°S (Fig. 8). This is because the SH midlatitude jet responds to increasing greenhouse gases on a much faster time scale than the thermodynamic processes that govern the global-mean surface temperature (Grise and Polvani 2017; Ceppi et al. 2018).

We find a stronger relationship between the global-mean surface temperature response (i.e., the climate sensitivity) and the sensitivity of midlatitude shortwave CRE to variations in near-surface temperature advection. Specifically, we find a significant correlation between ECS and the models' temperature advection sensitivity near 40°S in both CMIP5 and CMIP6 models, with models with more realistic representations of the observed shortwave CRE sensitivity to near-surface temperature advection generally having higher values of ECS (Figs. 9 and 10). Although the correlation is robust in both CMIP5 and CMIP6 models, correlations do not necessarily imply causality, and future research will be necessary to determine whether or not this linkage is physical in nature.

Overall, we conclude that constraining the sensitivities of models' CRE at midlatitudes to perturbations in EIS will help to improve the representation of the cloud radiative anomalies associated with midlatitude jet shifts (Fig. 7a), whereas constraining the sensitivities of models' CRE to perturbations in

near-surface temperature advection (particularly near 40°S) may help to reduce the uncertainty in ECS (Fig. 10a). We note that this conclusion is in some contrast to that of Zelinka et al. (2018), who found that the sensitivity of low cloud cover to perturbations in near-surface temperature advection over the North Pacific basin was more important for determining the cloud radiative anomalies associated with a North Pacific jet shift. Similar to the results shown in section 4 for the SH midlatitude jet, we have verified that the intermodel spread in the shortwave CRE anomalies (30°–60°N) associated with North Pacific jet shifts is significantly correlated with the models' sensitivities to perturbations in EIS, but not near-surface temperature advection (not shown). However, when focusing only on the easternmost North Pacific basin [as Zelinka et al. (2018) do], we do find a significant correlation between the shortwave CRE anomalies associated with North Pacific jet shifts and the models' sensitivities to perturbations in near-surface temperature advection, but only during summer months.

Zelinka et al. (2018) also conclude that the sensitivities of low cloud cover to perturbations in EIS and SST are more important for determining the climate change response, as the response of midlatitude near-surface temperature advection to climate change is smaller than that of the other cloud controlling factors (see Fig. 3 of Zelinka et al. 2020). Nevertheless, improving the sensitivity of models' CRE to short-term variability in temperature advection could still be important, as it may serve as an indirect proxy for other more direct processes that control ECS. The results of this study have revealed that CMIP6 models remain biased in how their midlatitude cloud radiative properties respond to variations in both EIS and near-surface temperature advection, and both Zelinka et al. (2018) and our study agree that improving these sensitivities will be important for more accurate modeling of the cloud radiative processes associated with midlatitude jet shifts and with climate change.

Acknowledgments. We thank Tim Myers and two anonymous reviewers for helpful comments. We acknowledge the World Climate Research Programme, which, through its Working Group on Coupled Modelling, coordinated and promoted CMIP6. We thank the climate modeling groups for producing and making available their model output, the Earth System Grid Federation (ESGF) for archiving the data and providing access, and the multiple funding agencies that support CMIP6 and ESGF. We would like to acknowledge high-performance computing support from Cheyenne (doi:10.5065/D6RX99HX) provided by NCAR's Computational and Information Systems Laboratory, sponsored by the National Science Foundation. This material is based upon work supported by the National Science Foundation under Grant AGS-1752900.

Data availability statement. All CMIP model output is freely and publicly available from Lawrence Livermore National Laboratory (WCRP 2011, 2019). Observational data used in this study are freely and publicly available from the NASA CERES Science Team (2020), Met Office Hadley Centre (2000), ECMWF (2017), and CFMIP (2011). Online locations for these data products are provided in the citations to these data sets in the references section below.

REFERENCES

Adam, O., and Coauthors, 2018a: TropD: Tropical width diagnostics software package, version 1.0. Zenodo, https://doi.org/10.5281/zenodo.1157043.

——, and Coauthors, 2018b: The TropD software package (v1): Standardized methods for calculating tropical-width diagnostics. *Geosci. Model Dev.*, **11**, 4339–4357, https://doi.org/10.5194/gmd-11-4339-2018.

Barnes, E. A., and L. Polvani, 2013: Response of the midlatitude jets, and of their variability, to increased greenhouse gases in the CMIP5 models. *J. Climate*, **26**, 7117–7135, https://doi.org/10.1175/JCLI-D-12-00536.1.

Bony, S., and J.-L. Dufresne, 2005: Marine boundary layer clouds at the heart of tropical cloud feedback uncertainties in climate models. *Geophys. Res. Lett.*, **32**, L20806, https://doi.org/10.1029/2005GL023851.

——, and Coauthors, 2006: How well do we understand and evaluate climate change feedback processes? *J. Climate*, **19**, 3445–3482, https://doi.org/10.1175/JCLI3819.1.

Boucher, O., and Coauthors, 2013: Clouds and aerosols. *Climate Change 2013: The Physical Science Basis*, T. F. Stocker et al., Eds., Cambridge University Press, 571–657.

Ceppi, P., and D. L. Hartmann, 2015: Connections between clouds, radiation, and midlatitude dynamics: A review. *Curr. Climate Change Rep.*, **1**, 94–102, https://doi.org/10.1007/s40641-015-0010-x.

——, G. Zappa, T. G. Shepherd, and J. M. Gregory, 2018: Fast and slow components of the extratropical atmospheric circulation response to CO_2 forcing. *J. Climate*, **31**, 1091–1105, https://doi.org/10.1175/JCLI-D-17-0323.1.

CERES Science Team, 2020: CERES_EBAF_Ed4.1 data quality summary. NASA, 27 pp., https://ceres.larc.nasa.gov/documents/DQ_summaries/CERES_EBAF_Ed4.1_DQS.pdf.

CFMIP, 2011: GCM Simulator-oriented ISCCP cloud product. L'Institut Pierre-Simon Laplace (IPSL), accessed 29 October 2013, https://climserv.ipsl.polytechnique.fr/cfmip-obs/.

Ciasto, L. M., and D. W. J. Thompson, 2008: Observations of large-scale ocean–atmosphere interaction in the Southern Hemisphere. *J. Climate*, **21**, 1244–1259, https://doi.org/10.1175/2007JCLI1809.1.

Dufresne, J.-L., and S. Bony, 2008: An assessment of the primary sources of spread of global warming estimates from coupled atmosphere–ocean models. *J. Climate*, **21**, 5135–5144, https://doi.org/10.1175/2008JCLI2239.1.

ECMWF, 2017: ERA5 Reanalysis. National Center for Atmospheric Research, Computational and Information Systems Laboratory, accessed 31 July 2020, https://doi.org/10.5065/D6X34W69.

Eyring, V., S. Bony, G. A. Meehl, C. A. Senior, B. Stevens, R. J. Stouffer, and K. E. Taylor, 2016: Overview of the Coupled Model Intercomparison Project Phase 6 (CMIP6) experimental design and organization. *Geosci. Model Dev.*, **9**, 1937–1958, https://doi.org/10.5194/gmd-9-1937-2016.

Field, P. R., and R. Wood, 2007: Precipitation and cloud structure in midlatitude cyclones. *J. Climate*, **20**, 233–254, https://doi.org/10.1175/JCLI3998.1.

Frey, W. R., and J. E. Kay, 2018: The influence of extratropical cloud phase and amount feedbacks on climate sensitivity. *Climate Dyn.*, **50**, 3097–3116, https://doi.org/10.1007/s00382-017-3796-5.

Georgakakos, K., and R. Bras, 1984: A hydrologically useful station precipitation model. 1. Formulation. *Water Resour. Res.*, **20**, 1585–1596, https://doi.org/10.1029/WR020i011p01585.

Gordon, N. D., and S. A. Klein, 2014: Low-cloud optical depth feedback in climate models. *J. Geophys. Res. Atmos.*, **119**, 6052–6065, https://doi.org/10.1002/2013JD021052.

——, J. R. Norris, C. P. Weaver, and S. A. Klein, 2005: Cluster analysis of cloud regimes and characteristic dynamics of midlatitude synoptic systems in observations and a model. *J. Geophys. Res.*, **110**, D15S17, https://doi.org/10.1029/2004JD005027.

Grise, K. M., and L. M. Polvani, 2014: Southern Hemisphere cloud-dynamics biases in CMIP5 models and their implications for climate projections. *J. Climate*, **27**, 6074–6092, https://doi.org/10.1175/JCLI-D-14-00113.1.

——, and B. Medeiros, 2016: Understanding the varied influence of midlatitude jet position on clouds and cloud-radiative effects in observations and global climate models. *J. Climate*, **29**, 9005–9025, https://doi.org/10.1175/JCLI-D-16-0295.1.

——, and L. M. Polvani, 2016: Is climate sensitivity related to dynamical sensitivity? *J. Geophys. Res. Atmos.*, **121**, 5159–5176, https://doi.org/10.1002/2015JD024687.

——, and ——, 2017: Understanding the time scales of the tropospheric circulation response to abrupt CO_2 forcing in the Southern Hemisphere: Seasonality and the role of the stratosphere. *J. Climate*, **30**, 8497–8515, https://doi.org/10.1175/JCLI-D-16-0849.1.

——, ——, G. Tselioudis, Y. Wu, and M. D. Zelinka, 2013: The ozone hole indirect effect: Cloud-radiative anomalies accompanying the poleward shift of the eddy-driven jet in the Southern Hemisphere. *Geophys. Res. Lett.*, **40**, 3688–3692, https://doi.org/10.1002/grl.50675.

Hersbach, H., and Coauthors, 2020: The ERA5 global reanalysis. *Quart. J. Roy. Meteor. Soc.*, **146**, 1999–2049, https://doi.org/10.1002/qj.3803.

Karpechko, A. Y., N. P. Gillett, G. J. Marshall, and J. A. Screen, 2009: Climate impacts of the southern annular mode simulated by the CMIP3 models. *J. Climate*, **22**, 3751–3768, https://doi.org/10.1175/2009JCLI2788.1.

Kawai, H., T. Koshiro, and M. J. Webb, 2017: Interpretation of factors controlling low cloud cover and low cloud feedback using a unified predictive index. *J. Climate*, **30**, 9119–9131, https://doi.org/10.1175/JCLI-D-16-0825.1.

Kay, J. E., B. Medeiros, Y.-T. Hwang, A. Gettelman, J. Perket, and M. G. Flanner, 2014: Processes controlling Southern Ocean shortwave climate feedbacks in CESM. *Geophys. Res. Lett.*, **41**, 616–622, https://doi.org/10.1002/2013GL058315.

Kelleher, M. K., and K. M. Grise, 2019: Examining Southern Ocean cloud controlling factors on daily time scales and their connections to midlatitude weather systems. *J. Climate*, **32**, 5145–5160, https://doi.org/10.1175/JCLI-D-18-0840.1.

Klein, S. A., and D. L. Hartmann, 1993: The seasonal cycle of low stratiform clouds. *J. Climate*, **6**, 1587–1606, https://doi.org/10.1175/1520-0442(1993)006<1587:TSCOLS>2.0.CO;2.

——, A. Hall, J. R. Norris, and R. Pincus, 2017: Low-cloud feedbacks from cloud-controlling factors: A review. *Surv. Geophys.*, **38**, 1307–1329, https://doi.org/10.1007/s10712-017-9433-3.

Lau, N.-C., and M. W. Crane, 1995: A satellite view of the synoptic-scale organization of cloud properties in midlatitude and tropical circulation systems. *Mon. Wea. Rev.*, **123**, 1984–2006, https://doi.org/10.1175/1520-0493(1995)123<1984:ASVOTS>2.0.CO;2.

——, and ——, 1997: Comparing satellite and surface observations of cloud patterns in synoptic-scale circulation systems. *Mon. Wea. Rev.*, **125**, 3172–3189, https://doi.org/10.1175/1520-0493(1997)125<3172:CSASOO>2.0.CO;2.

Li, Y., D. W. J. Thompson, G. L. Stephens, and S. Bony, 2014: A global survey of the instantaneous linkages between cloud vertical structure and large-scale climate. *J. Geophys. Res. Atmos.*, **119**, 3770–3792, https://doi.org/10.1002/2013JD020669.

Loeb, N. G., and Coauthors, 2018: Clouds and the Earth's Radiant Energy System (CERES) Energy Balanced and Filled (EBAF) top-of-atmosphere (TOA) edition-4.0 data product. *J. Climate*, **31**, 895–918, https://doi.org/10.1175/JCLI-D-17-0208.1.

McCoy, D. T., I. Tan, D. L. Hartmann, M. D. Zelinka, and T. Storelvmo, 2016: On the relationships among cloud cover, mixed-phase partitioning, and planetary albedo in GCMs. *J. Adv. Model. Earth Syst.*, **8**, 650–668, https://doi.org/10.1002/2015MS000589.

——, R. Eastman, D. L. Hartmann, and R. Wood, 2017: The change in low cloud cover in a warmed climate inferred from AIRS, MODIS, and ERA-Interim. *J. Climate*, **30**, 3609–3620, https://doi.org/10.1175/JCLI-D-15-0734.1.

——, P. Field, A. Bodas-Salcedo, G. S. Elsaesser, and M. D. Zelinka, 2020: A regime-oriented approach to observationally constraining extratropical shortwave cloud feedbacks. *J. Climate*, **33**, 9967–9983, https://doi.org/10.1175/JCLI-D-19-0987.1.

Meehl, G. A., C. A. Senior, V. Eyring, G. Flato, J.-F. Lamarque, R. J. Stouffer, K. E. Taylor, and M. Schlund, 2020: Context for interpreting equilibrium climate sensitivity and transient climate response from the CMIP6 Earth system models. *Sci. Adv.*, **6**, eaba1981, https://doi.org/10.1126/sciadv.aba1981.

Met Office Hadley Centre, 2000: Hadley Centre Global Sea Ice and Sea Surface Temperature (HadISST), version 1.1. Met Office Hadley Centre, accessed 31 July 2020, https://www.metoffice.gov.uk/hadobs/hadisst.

Miyamoto, A., H. Nakamura, and T. Miyasaka, 2018: Influence of the subtropical high and storm track on low-cloud fraction and its seasonality over the south Indian Ocean. *J. Climate*, **31**, 4017–4039, https://doi.org/10.1175/JCLI-D-17-0229.1.

Morcrette, J.-J., and Y. Fouquart, 1986: The overlapping of cloud layers in shortwave radiation parameterizations. *J. Atmos. Sci.*, **43**, 321–328, https://doi.org/10.1175/1520-0469(1986)043<0321:TOOCLI>2.0.CO;2.

Myers, T. A., and J. R. Norris, 2013: Observational evidence that enhanced subsidence reduces subtropical marine boundary layer cloudiness. *J. Climate*, **26**, 7507–7524, https://doi.org/10.1175/JCLI-D-12-00736.1.

——, and ——, 2015: On the relationships between subtropical clouds and meteorology in observations and CMIP3 and CMIP5 models. *J. Climate*, **28**, 2945–2967, https://doi.org/10.1175/JCLI-D-14-00475.1.

——, and ——, 2016: Reducing the uncertainty in subtropical cloud feedback. *Geophys. Res. Lett.*, **43**, 2144–2148, https://doi.org/10.1002/2015GL067416.

Norris, J. R., and C. P. Weaver, 2001: Improved techniques for evaluating GCM cloudiness applied to the NCAR CCM3. *J. Climate*, **14**, 2540–2550, https://doi.org/10.1175/1520-0442(2001)014<2540:ITFEGC>2.0.CO;2.

——, and S. F. Iacobellis, 2005: North Pacific cloud feedbacks inferred from synoptic-scale dynamic and thermodynamic relationships. *J. Climate*, **18**, 4862–4878, https://doi.org/10.1175/JCLI3558.1.

Pincus, R., S. Platnick, S. A. Ackerman, R. S. Hemler, and R. J. P. Hoffmann, 2012: Reconciling simulated and observed views of clouds: MODIS, ISCCP, and the limits of instrument simulators.

J. Climate, **25**, 4699–4720, https://doi.org/10.1175/JCLI-D-11-00267.1.

Qu, X., A. Hall, S. A. Klein, and P. M. Caldwell, 2014: On the spread of changes in marine low cloud cover in climate model simulations of the 21st century. *Climate Dyn.*, **42**, 2603–2626, https://doi.org/10.1007/s00382-013-1945-z.

——, ——, ——, and A. M. DeAngelis, 2015: Positive tropical marine low-cloud cover feedback inferred from cloud-controlling factors. *Geophys. Res. Lett.*, **42**, 7767–7775, https://doi.org/10.1002/2015GL065627.

Ramanathan, V., R. D. Cess, E. F. Harrison, P. Minnis, B. R. Barkstrom, E. Ahmad, and D. Hartmann, 1989: Cloud-radiative forcing and climate: Results from the Earth Radiation Budget Experiment. *Science*, **243**, 57–63, https://doi.org/10.1126/science.243.4887.57.

Rayner, N. A., D. E. Parker, E. B. Horton, C. K. Folland, L. V. Alexander, D. P. Rowell, E. C. Kent, and A. Kaplan, 2003: Global analyses of sea surface temperature, sea ice, and night marine air temperature since the late nineteenth century. *J. Geophys. Res.*, **108**, 4407, https://doi.org/10.1029/2002JD002670.

Rieck, M., L. Nuijens, and B. Stevens, 2012: Marine boundary layer cloud feedbacks in a constant relative humidity atmosphere. *J. Atmos. Sci.*, **69**, 2538–2550, https://doi.org/10.1175/JAS-D-11-0203.1.

Scott, R. C., T. A. Myers, J. R. Norris, M. D. Zelinka, S. A. Klein, M. Sun, and D. R. Doelling, 2020: Observed sensitivity of low-cloud radiative effects to meteorological perturbations over the global oceans. *J. Climate*, **33**, 7717–7734, https://doi.org/10.1175/JCLI-D-19-1028.1.

Screen, J. A., N. P. Gillett, A. Y. Karpechko, and D. P. Stevens, 2010: Mixed layer temperature response to the southern annular mode: Mechanisms and model representation. *J. Climate*, **23**, 664–678, https://doi.org/10.1175/2009JCLI2976.1.

Seethala, C., J. R. Norris, and T. A. Myers, 2015: How has subtropical stratocumulus and associated meteorology changed since the 1980s? *J. Climate*, **28**, 8396–8410, https://doi.org/10.1175/JCLI-D-15-0120.1.

Sen Gupta, A., and M. H. England, 2006: Coupled ocean–atmosphere–ice response to variations in the southern annular mode. *J. Climate*, **19**, 4457–4486, https://doi.org/10.1175/JCLI3843.1.

Soden, B. J., and G. A. Vecchi, 2011: The vertical distribution of cloud feedback in coupled ocean–atmosphere models. *Geophys. Res. Lett.*, **38**, L12704, https://doi.org/10.1029/2011GL047632.

Tan, I., T. Storelvmo, and M. D. Zelinka, 2016: Observational constraints on mixed-phase clouds imply higher climate sensitivity. *Science*, **352**, 224–227, https://doi.org/10.1126/science.aad5300.

Taylor, K. E., R. J. Stouffer, and G. A. Meehl, 2012: An overview of CMIP5 and the experiment design. *Bull. Amer. Meteor. Soc.*, **93**, 485–498, https://doi.org/10.1175/BAMS-D-11-00094.1.

Terai, C. R., M. Zelinka, and S. A. Klein, 2016: Constraining the low-cloud optical depth feedback at middle and high latitudes using satellite observations. *J. Geophys. Res. Atmos.*, **121**, 9696–9716, https://doi.org/10.1002/2016JD025233.

Vallis, G. K., P. Zurita-Gotor, C. Cairns, and J. Kidston, 2015: Response of the large-scale structure of the atmosphere to global warming. *Quart. J. Roy. Meteor. Soc.*, **141**, 1479–1501, https://doi.org/10.1002/qj.2456.

Vial, J., J.-L. Dufresne, and S. Bony, 2013: On the interpretation of inter-model spread in CMIP5 climate sensitivity estimates. *Climate Dyn.*, **41**, 3339–3362, https://doi.org/10.1007/s00382-013-1725-9.

Wall, C. J., and D. L. Hartmann, 2015: On the influence of poleward jet shift on shortwave cloud feedback in global climate models. *J. Adv. Model. Earth Syst.*, **7**, 2044–2059, https://doi.org/10.1002/2015MS000520.

——, ——, and P. Ma, 2017: Instantaneous linkages between clouds and large-scale meteorology over the Southern Ocean in observations and a climate model. *J. Climate*, **30**, 9455–9474, https://doi.org/10.1175/JCLI-D-17-0156.1.

WCRP, 2011: Coupled Model Intercomparison Project, phase 5. Lawrence Livermore National Laboratory, accessed 7 March 2018, https://esgf-node.llnl.gov/search/cmip5/.

——, 2019: Coupled Model Intercomparison Project, phase 6. Lawrence Livermore National Laboratory, accessed 2 July 2020, https://esgf-node.llnl.gov/search/cmip6/.

Weare, B. C., 2000: Near-global observations of low clouds. *J. Climate*, **13**, 1255–1268, https://doi.org/10.1175/1520-0442(2000)013<1255:NGOOLC>2.0.CO;2.

Weaver, C. P., and V. Ramanathan, 1997: Relationships between large-scale vertical velocity, static stability, and cloud radiative forcing over Northern Hemisphere extratropical oceans. *J. Climate*, **10**, 2871–2887, https://doi.org/10.1175/1520-0442(1997)010<2871:RBLSVV>2.0.CO;2.

Webb, M. J., F. H. Lambert, and J. M. Gregory, 2013: Origins of differences in climate sensitivity, forcing and feedback in climate models. *Climate Dyn.*, **40**, 677–707, https://doi.org/10.1007/s00382-012-1336-x.

Wilks, D. S., 2016: "The stippling shows statistically significant grid points": How research results are routinely overstated and overinterpreted, and what to do about it. *Bull. Amer. Meteor. Soc.*, **97**, 2263–2273, https://doi.org/10.1175/BAMS-D-15-00267.1.

Wood, R., and C. S. Bretherton, 2006: On the relationship between stratiform low cloud cover and lower-tropospheric stability. *J. Climate*, **19**, 6425–6432, https://doi.org/10.1175/JCLI3988.1.

Zelinka, M. D., K. M. Grise, S. A. Klein, C. Zhou, A. M. DeAngelis, and M. W. Christensen, 2018: Drivers of the low-cloud response to poleward jet shifts in the North Pacific in observations and models. *J. Climate*, **31**, 7925–7947, https://doi.org/10.1175/JCLI-D-18-0114.1.

——, T. A. Myers, D. T. McCoy, S. Po-Chedley, P. M. Caldwell, P. Ceppi, S. A. Klein, and K. E. Taylor, 2020: Causes of higher climate sensitivity in CMIP6 models. *Geophys. Res. Lett.*, **47**, e2019GL085782, https://doi.org/10.1029/2019GL08578.

Zhang, Y., and Coauthors, 2012: Regional assessment of the parameter-dependent performance of CAM4 in simulating tropical clouds. *Geophys. Res. Lett.*, **39**, L14708, https://doi.org/10.1029/2012GL052184.